Dimensional crossover of Bose-Einstein-condensation phenomena in quantum gases confined within slab geometries

Francesco Delfino and Ettore Vicari
Dipartimento di Fisica dell'Università di Pisa and INFN, Largo Pontecorvo 3, I-56127 Pisa, Italy
(Received 1 July 2017; revised manuscript received 22 August 2017; published 23 October 2017)

We investigate systems of interacting bosonic particles confined within slablike boxes of size $L^2 \times Z$ with $Z \ll L$, at their three-dimensional (3D) Bose-Einstein-condensation (BEC) transition temperature T_c, and below T_c where they experience a quasi-two-dimensional (quasi-2D) Berezinskii-Kosterlitz-Thouless (BKT) transition (at $T_{\rm BKT} < T_c$ depending on the thickness Z). The low-temperature phase below $T_{\rm BKT}$ shows quasi-long-range order: the planar correlations decay algebraically as predicted by the 2D spin-wave theory. This dimensional crossover, from a 3D behavior for $T \gtrsim T_c$ to a quasi-2D critical behavior for $T \lesssim T_{\rm BKT}$, can be described by a transverse finite-size scaling limit in a slab geometry. Numerical evidence of the 3D $\to$ 2D dimensional crossover is presented for the Bose-Hubbard model defined in anisotropic $L^2 \times Z$ lattices with $Z \ll L$. We extend this scaling analysis to the case the slab geometry of the gas is effectively realized by a transverse (inhomogeneous) harmonic trap. Finally, we discuss off-equilibrium behaviors arising from slow time variations of the temperature across the BEC transition of gases confined within a slab geometry. We argue that the system develops an off-equilibrium transverse finite-size scaling under these time-dependent protocols.

DOI: 10.1103/PhysRevA.96.043623

I. INTRODUCTION

The Bose-Einstein condensation (BEC) characterizes the low-temperature behavior of three-dimensional (3D) bosonic gases, below a finite-temperature BEC phase transition separating the high-temperature normal phase and the low-temperature superfluid BEC phase. The phase coherence properties of the BEC phase have been observed by several experiments (see, e.g., Refs. [1–10]). Several theoretical and experimental studies have also investigated the critical properties at the BEC transition, when the condensate begins forming (see, e.g., Refs. [11–33]). Both the phase-coherence properties of the BEC phase and the critical behavior at the BEC transition turn out to be particularly sensitive to the inhomogeneous conditions arising from the presence of spatially dependent confining potentials, and/or the geometry of the atomic-gas system. Inhomogeneous conditions due to space-dependent trapping potentials give rise to a universal distortion of the homogeneous critical behavior, which can be cast in terms of a universal trap-size scaling [14,26] controlled by the same universality class of the 3D BEC transition. In the case of homogeneous traps, such as those experimentally realized in Refs. [28,30,31,33], the geometry of the trap may lead to quite different phase-coherence properties, when passing from 3D to quasi-two-dimensional (quasi-2D) or quasi-one-dimensional (quasi-1D) systems. For example, atomic gases in elongated homogeneous boxes [34] and harmonic traps [6,7,35–38] show a spatial dimensional crossover from a high-temperature 3D behavior to a low-temperature quasi-1D behavior.

In this paper, we consider bosonic particle systems confined within a slablike geometry, i.e., within boxes of size $L^2 \times Z$ with $Z \ll L$. We investigate their behavior at the BEC transition temperature T_c (this is the critical temperature of the 3D system in the thermodynamic limit, i.e., when all system sizes tend to infinity) and at lower temperatures. Their low-temperature behavior ($T < T_c$) is further characterized by the possibility of undergoing a finite-temperature transition to a quasi-long-range-order (QLRO) phase, with long-range planar correlations which decay algebraically. This is the well-known Berezinskii-Kosterlitz-Thouless (BKT) transition [39–42], which occurs in 2D systems with a global U(1) symmetry. Experimental evidences of BKT transitions have been also reported for quasi-2D trapped atomic gases [43–49].

The behavior of homogeneous gases confined within a slab geometry shows dimensional crossover (DC) from a 3D behavior for $T \gtrsim T_c$ to a quasi-2D critical behavior for $T \lesssim T_{\rm BKT}$. In the limit of large thickness Z, the quasi-2D BKT transition temperature approaches that of the 3D BEC transition, i.e., $T_{\rm BKT} \to T_c^-$ for $Z \to \infty$ (assuming the thermodynamic limit for the planar directions, i.e., $L \gg Z$). The interplay of the BEC and BKT critical modes gives rise to a quite complex behavior. We show that it can be described by a transverse finite-size scaling (TFSS) limit for systems confined within a slab geometry [50,51], i.e., $Z \to \infty$ and $T \to T_c$ keeping the product $(T - T_c)Z^{1/\nu}$ fixed, where ν is the correlation-length exponent at the 3D BEC transition. In this TFSS limit, the BKT transition below T_c appears as an essential singularity of the TFSS functions.

The DC scenario is expected to apply to any quantum gas of interacting bosonic particles confined in boxes or lattice structures with a slab geometry. The DC scenario is supported by a numerical study of the Bose-Hubbard (BH) model [52], which models bosonic atoms in optical lattices [10,53]. We show that the predictions of the 3D $\to$ 2D DC are realized when considering anisotropic slablike lattices $L^2 \times Z$ with $Z \ll L$.

We mention that DC phenomena have been also investigated in ^{4}He systems in film geometries [54], and 3D XY spin models defined in slablike lattices [55–58], whose phase transitions belong to the same universality class of the BEC transition.

The DC scenario also arises when the slab geometry is realized by trapping the particles by an external (inhomogeneous)

harmonic potential. The corresponding scaling behaviors can be inferred using the trap-size scaling framework [14,26].

We also extend the discussion to the off-equilibrium behavior arising from slow time variations of the temperature across the BEC transition. The behavior of weakly interacting atomic gas confined in quasi-2D geometries has been experimentally investigated under time-dependent protocols across the BEC regime (see, e.g., Refs. [31,33]) to verify the Kibble-Zurek mechanism of defect production [59,60]. In gases confined within a slab geometry, the off-equilibrium behavior arising from the slow variation of the temperature across the BEC transition point is made particularly complex by the presence of the quasi-2D BKT transition at $T_{\rm BKT} \lesssim T_c$. Thus, disentangling the behaviors corresponding to 3D BEC and quasi-2D BKT transitions may be quite hard in experimental or numerical analyses. To describe this complex behavior, we put forward an off-equilibrium TFSS framework for bosonic gases confined within slablike homogeneous traps.

The paper is organized as follows. In Sec. II, we introduce the BH model that we use as a paradigmatic model of Bose gases showing the DC phenomenon when confined within a slab geometry; we also define the observables that we consider in the rest of the paper. In Sec. III, we present the general features of the DC of Bose gases confined in a slab geometry, exploiting the framework provided by the TFSS theory. In Sec. IV, we present a numerical study of the DC scaling behavior in 3D BH models. In Sec. V, we discuss the new features arising when the confinement of the particles along the transverse direction is due to a harmonic trap. In Sec. VI, we study the off-equilibrium behavior arising from slow time variations of the temperature across the BEC transition, and put forward the corresponding off-equilibrium scaling ansatz. Finally, we summarize our results in Sec. VII. We also add a few appendices. Appendix A reports some exact spin-wave results for the phase-coherence correlations within the low-temperature phase of quasi-2D bosonic systems. In Appendix B we discuss the critical behavior arising at the boundary of the BEC region in Bose gases trapped by a transverse harmonic potential.

II. BOSE-HUBBARD MODEL IN A SLAB GEOMETRY

Lattice BH models [52] are interesting examples of interacting Bose gases undergoing BEC transitions. They provide realistic models of gases of bosonic atoms in optical lattices [53]. In the following discussions, we use the BH model as a paradigmatic model of Bose gases showing DC in a slab geometry.

The Hamiltonian of BH models reads as

$$H_{\rm BH} = -t \sum_{\langle ij \rangle} (b_i^\dagger b_j + b_j^\dagger b_i) + \frac{U}{2} \sum_i n_i(n_i - 1) - \mu \sum_i n_i \,, \qquad (1)$$

where b_i is a bosonic operator, $n_i \equiv b_i^\dagger b_i$ is the particle density operator, the sums run over the bonds $\langle ij \rangle$ and the sites i of a cubic $L_1 \times L_2 \times L_3$ lattice, $a = 1$ is the lattice spacing (thus lengths are expressed in units of a). The phase coherence properties can be inferred from the one-particle correlation function

$$G(\boldsymbol{r}_1, \boldsymbol{r}_2) \equiv \frac{{\rm Tr}\, b_{\boldsymbol{r}_1}^\dagger b_{\boldsymbol{r}_2} e^{-H_{\rm BH}/T}}{{\rm Tr}\, e^{-H_{\rm BH}/T}}. \qquad (2)$$

We set the hopping parameter $t = 1$, so that all energies are expressed in units of t, and the Planck constant $\hbar = 1$.

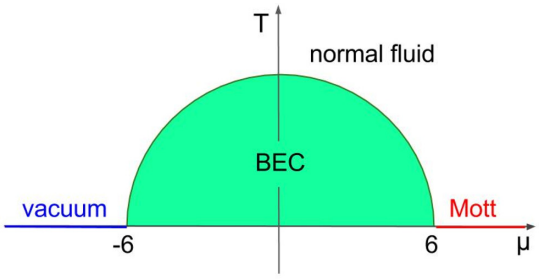

FIG. 1. Sketch of the T-μ (in units of the hopping parameter t) phase diagram of the 3D BH model in the hard-core $U \to \infty$ limit. The BEC phase is restricted to a finite region between $\mu = -6$ and 6. It is bounded by a BEC transition line $T_c(\mu)$, which satisfies $T_c(\mu) = T_c(-\mu)$ due to a particle-hole symmetry. Its maximum occurs at $\mu = 0$, where [27,29] $T_c(\mu = 0) = 2.01599(5)$; we also know that [26] $T_c(\mu \pm 4) = 1.4820(2)$. At $T = 0$, two further quantum phases exist: the vacuum phase ($\mu < -6$) and the incompressible $n = 1$ Mott phase ($\mu > 6$). Since we set $t = 1$ for the hopping parameter of the BH model (1), T and μ are expressed in units of t.

The phase diagram of 3D BH models and their critical behaviors have been much investigated (see, e.g., Refs. [25–27,29,52,61]). Their T-μ phase diagram presents a finite-temperature BEC transition line. This is characterized by the accumulation of a macroscopic number of atoms in a single quantum state, which gives rise to a phase-coherent condensate. See, for example, Fig. 1, which shows a sketch of the phase diagram of 3D BH models in the hard-core $U \to \infty$ limit, where the occupation site number is limited to the cases $n = 0, 1$. The condensate wave function provides the complex order parameter of the BEC transition, whose critical behavior belongs to the U(1)-symmetric XY universality class. This implies that the length scale ξ of the critical modes diverges at T_c as [62–68]

$$\xi \sim (T - T_c)^{-\nu}, \quad \nu = 0.6717(1). \qquad (3)$$

This has been accurately verified by numerical studies (see, e.g., Refs. [25–27,29]). The BEC phase extends below the BEC transition line. In particular, in the hard-core limit $U \to \infty$ and for $\mu = 0$ (corresponding to half-filling), the BEC transition occurs at [27,29] $T_c = 2.01599(5)$.

We consider BH lattice gases in anisotropic slablike geometries, i.e., $L^2 \times Z$ lattices with $Z \ll L$. We consider open boundary conditions (OBC) along the transverse Z direction; we label the corresponding coordinate as $-(Z-1)/2 \leqslant z \leqslant (Z-1)/2$, so that the innermost plane is the $z = 0$ plane (see Fig. 2). This choice is motivated by the fact that OBC corresponds to gas systems trapped by hard walls, such as the experimental systems of Refs. [28,30,31,33]. Since the thickness Z of the slab is generally considered as much smaller than the size L of the planar directions, and in most cases we consider the 2D *thermodynamic* $L \to \infty$ limit keeping

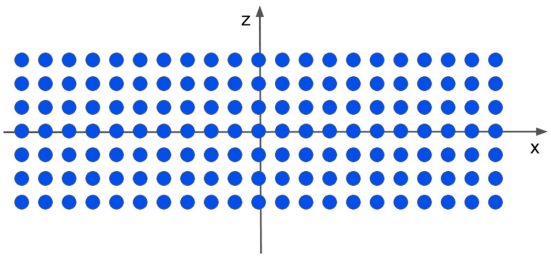

FIG. 2. Sketch of the $L^2 \times Z$ slab geometry with $L \gg Z$. The figure shows a slice of the lattice system on the x-z plane (the y direction runs orthogonal to the x-z plane, along which the system extends analogously to the x direction). The blobs indicate the lattice sites whose integer coordinates are limited by $1 \leqslant x,y \leqslant L$ and $-(Z-1)/2 \leqslant z \leqslant (Z-1)/2$. The one-particle correlation function $g(\boldsymbol{x})$ [cf. Eq. (4)] and the corresponding correlation length ξ [cf. Eq. (6)] are defined along the $z = 0$ plane.

Z fixed, the boundary conditions along the planar directions are generally irrelevant for our study around T_c. However, they become relevant at the BKT transition where the planar correlation length diverges. In the following, we consider the most convenient periodic boundary conditions (PBC) along the large planar dimensions; the corresponding site coordinates are $\boldsymbol{x} = (x_1,x_2)$ with $x_{1,2} = 1,\ldots,L$.

We want to understand how the phase diagram and critical behavior change when varying the thickness Z. As we shall argue, BH systems below T_c are expected to develop quasi-2D critical modes, leading to a BKT transition with a diverging planar correlation length, and a low-temperature QLRO phase.

To study this phenomenon, and in particular how the $Z \to \infty$ limit eventually realizes the 3D critical behavior at T_c, we focus on the behavior of the correlation function (2) along the planar directions. In particular, for simplicity reasons, we study the correlation function between points belonging to the central $z = 0$ plane, i.e.,

$$g(\boldsymbol{x}_1 - \boldsymbol{x}_2) \equiv G[(\boldsymbol{x}_1,0),(\boldsymbol{x}_2,0)], \tag{4}$$

where we have taken into account the invariance of the system for translations along the $\hat{x}$ and $\hat{y}$ directions. In particular, we consider the corresponding *planar susceptibility*

$$\chi = \sum_{\boldsymbol{x}} g(\boldsymbol{x}), \tag{5}$$

where the sum is over the sites $\boldsymbol{x}$ of the central plane, and *planar second-moment correlation length* ξ

$$\xi^2 = \frac{1}{4\chi} \sum_{\boldsymbol{x}} \boldsymbol{x}^2 g(\boldsymbol{x}). \tag{6}$$

More precisely, since we consider PBC along the planar directions, we use the equivalent definition

$$\xi^2 \equiv \frac{1}{4\sin^2(\pi/L)} \frac{\tilde{g}(\boldsymbol{0}) - \tilde{g}(\boldsymbol{p})}{\tilde{g}(\boldsymbol{p})}, \tag{7}$$

where $\tilde{g}(\boldsymbol{p})$ is the 2D Fourier transform of $g(\boldsymbol{x})$, and $\boldsymbol{p} = (2\pi/L,0)$.

The helicity modulus Υ is a measure of the response of the system to a phase-twisting field along one of the lattice directions [69]. In the case of bosonic systems, it is related to the superfluid density [34,69,70]. We consider the helicity modulus along the planar directions $\hat{x}$ and $\hat{y}$, i.e.,

$$\Upsilon_a \equiv \frac{1}{Z} \frac{\partial^2 F(\phi_a)}{\partial \phi_a^2}\bigg|_{\phi_a=0} \equiv \frac{T}{Z} Y_a, \tag{8}$$

where $F = -T \ln Z$ is the free energy, ϕ_a are twist angles along one of the planar directions. Note that $Y_1 = Y_2$ by symmetry for $L^2 \times Z$ systems.

As we shall see, the quantities

$$Y \equiv Y_a, \quad R_L \equiv \xi/L \tag{9}$$

are particularly useful to check the effective spin-wave behavior along the planar directions for $T \leqslant T_{\rm BKT} < T_c$.

III. DIMENSIONAL CROSSOVER OF BOSE GASES IN A SLAB GEOMETRY

A. Phase diagram for a finite thickness Z

The 3D scenario sketched in Fig. 1 substantially changes if we consider a quasi-2D thermodynamic limit, i.e., $L \to \infty$ keeping Z fixed. Indeed, the length scale ξ remains finite at the BEC transition point when Z is kept fixed. Of course, the full 3D critical behavior must be somehow recovered when $Z \to \infty$, for which one expects $\xi(Z) \sim Z$. More precisely, defining

$$R_Z = \lim_{L\to\infty} \xi/Z, \tag{10}$$

standard FSS arguments [50,51] predict that at the 3D critical point T_c

$$R_Z(T_c) = R_Z^* + O(Z^{-\omega}), \tag{11}$$

where R_Z^* is a universal constant and $\omega = 0.785(20)$ is the scaling-correction exponent associated with the leading irrelevant perturbation at the XY fixed point [62,64,66]. Note that the universal constant R_Z^* depends on the boundary conditions along the transverse direction (the boundary conditions along the planar directions are irrelevant since we assume $L \gg Z$ and $\xi \sim Z$).

However, we should also take into account that 2D or quasi-2D systems with a global U(1) symmetry may undergo a finite-temperature transition described by the BKT theory [39–42]. The BKT transition separates a high-temperature normal phase and a low-temperature phase characterized by QLRO, where correlations decay algebraically at large distances, without the emergence of a nonvanishing order parameter [71,72]. When approaching the BKT transition point $T_{\rm BKT}$ from the high-temperature normal phase, these systems develop an exponentially divergent correlation length:

$$\xi \sim \exp(c/\sqrt{\tau}), \quad \tau \equiv T/T_{\rm BKT} - 1, \tag{12}$$

where c is a nonuniversal constant. The magnetic susceptibility diverges as $\chi \sim \xi^{7/4}$, corresponding to the critical exponent $\eta = \frac{1}{4}$ controlling the critical behavior of the two-point correlation function at the BKT transition [73].

Consistently with the above picture, 2D BH systems [corresponding to the Hamiltonian (1) with $Z = 1$] undergo a BKT transition. Figure 3 shows a sketch of the phase diagram of 2D BH systems in the hard-core $U \to \infty$ limit. The finite-temperature BKT transition of BH models has

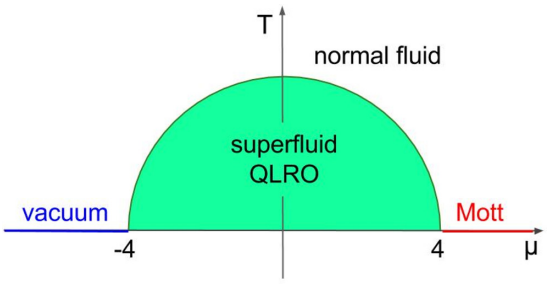

FIG. 3. Sketch of the phase diagram of the 2D BH model in the hard-core $U \to \infty$ limit. The normal and superfluid QLRO phases are separated by a finite-temperature BKT transition line, which satisfies $T_{\rm BKT}(\mu) = T_{\rm BKT}(-\mu)$ due to a particle-hole symmetry. Its maximum occurs at $\mu = 0$, where [73] $T_{\rm BKT}(\mu = 0) = 0.6877(2)$. The superfluid QLRO phase is restricted to a finite region between $\mu = -4$ and 4, which is narrower than that of the 3D phase diagram (see Fig. 1). Since we set $t = 1$ for the hopping parameter of the BH model, T and μ are expressed in units of t.

been numerically investigated by several studies (see, e.g., Refs. [25,73–76]). In particular, $T_{\rm BKT} = 0.6877(2)$ in the hard-core $U \to \infty$ limit and for $\mu = 0$ [73]. Note that the 2D BH systems do not show a real BEC below the critical temperature $T_{\rm BKT}$, but QLRO where the phase-coherence correlations decay algebraically.

The phase diagram of quasi-2D systems with finite thickness $Z > 1$ is expected to be analogous to that of 2D BH systems, with a BKT transition at $T_{\rm BKT}$ depending on the thickness Z. Analogously to 2D systems, they are expected to show a QLRO phase below $T_{\rm BKT}$, where correlation functions show power-law decays along the planar directions, as described by the 2D spin-wave theory. In Appendix A, we summarize some exact results which are expected to characterize the low-temperature QLRO phase of quasi-2D interacting bosonic gases up to the BKT transition.

B. Dimensional crossover limit

The above scenario can be interpreted as a dimensional crossover (DC) from a 3D behavior when $T \gtrsim T_c$, and ξ is finite (in particular the anisotropy of the system is not locally relevant when $\xi \ll Z$), to an effective 2D critical behavior at $T \lesssim T_{\rm BKT}(Z)$ where the planar correlation length ξ diverges.

Such a DC can be described by an appropriate transverse finite-size scaling (TFSS) limit, defined as $\delta \equiv 1 - T/T_c \to 0$ and $Z \to \infty$, keeping $\delta Z^{1/\nu}$ fixed. In this TFSS limit [50,51]

$$R_Z \equiv \xi/Z \approx \mathcal{R}(X), \quad X = Z^{1/\nu}\delta, \tag{13}$$

where $\mathcal{R}(X)$ is a universal function (apart from a trivial normalization of the argument X), but depending on the boundary conditions along the Z direction. Scaling corrections are suppressed as $Z^{-\omega}$, analogously to Eq. (11).

In this TFSS framework, the BKT transition is expected to appear as an essential singularity of the scaling function $\mathcal{R}(X)$:

$$\mathcal{R}(X) \sim \exp\left(\frac{b}{\sqrt{X_{\rm BKT} - X}}\right) \quad \text{for} \quad X \to X_{\rm BKT}^-, \tag{14}$$

where $X_{\rm BKT}$ is the value of the scaling variable X corresponding to the BKT transition point

$$\delta_{\rm BKT}(Z) \equiv \frac{T_c - T_{\rm BKT}(Z)}{T_c}, \tag{15}$$

i.e.,

$$X_{\rm BKT} = \lim_{Z\to\infty} Z^{1/\nu}\delta_{\rm BKT}(Z) \ > 0. \tag{16}$$

The constant b in Eq. (14) is a nonuniversal constant depending on the normalization of the scaling variable X. $\mathcal{R}(X)$ is not defined for $X \geqslant X_{\rm BKT}$. Note that the above scaling equations predict that

$$\delta_{\rm BKT}(Z) \sim Z^{-1/\nu} \tag{17}$$

in the large-Z limit (see also Refs. [77–79] for analogous considerations applied to other physical systems).

The TFSS of the planar two-point function (4) is given by

$$g(\boldsymbol{x}, Z) \approx Z^{-(1+\eta)}\mathcal{G}(\boldsymbol{x}/Z, X), \tag{18}$$

where $\eta = 0.0381(2)$ is the critical exponent of the 3D XY universality class [64], associated with the power-law decay of the two-point function at T_c. Equation (18) also implies that the planar susceptibility defined as in Eq. (5) behaves as

$$\chi \approx Z^{1-\eta}\mathcal{C}(X). \tag{19}$$

It is important to note that the above features are shared with any quasi-2D system with a global U(1) symmetry, and in particular standard O(2)-symmetric spin models. Numerical analyses of DC issues for the XY model are reported in Refs. [55–58].

IV. NUMERICAL RESULTS FOR THE BH MODEL

In order to check the DC scenario discussed in the previous section, we present a numerical study of the equilibrium properties of the BH model (1) in the hard-core $U \to \infty$ limit and at zero chemical potential $\mu = 0$, corresponding to half-filling, i.e., $\langle n_{\boldsymbol{r}} \rangle = \frac{1}{2}$ for any T. In the hard-core limit and for $\mu = 0$, the 3D BEC transition occurs at $T_c = 2.01599(5)$ and the 2D BKT transition at $T_{\rm BKT} = 0.6877(2)$.

Numerical results are obtained by quantum Monte Carlo (QMC) simulations using the directed operator-loop algorithm [80–82]. As already mentioned in Sec. II, we consider a slab geometry, i.e., $L^2 \times Z$ lattices with $Z \ll L$, with OBC along the transverse directions, and PBC along the planar directions. We present numerical results for some values of the thickness Z, in particular, $Z = 5, 9, 13$, various planar sizes up to $L \approx 100$, and several values of the temperature $T \lesssim T_c$. The maximum size Z of our numerical study is limited by the fact that the computational effort of QMC rapidly increases because they also require larger values of the planar sizes.

We compute the observables defined in Sec. II. In QMC simulations, the helicity modulus is obtained from the linear winding number W_a along the ath direction, i.e.,

$$Y \equiv Y_a = \langle W_a^2 \rangle, \quad W_a = \frac{N_a^+ - N_a^-}{L}, \tag{20}$$

where N_a^+ and N_a^- are the numbers of nondiagonal operators which move the particles, respectively, in the positive and negative ath direction.

Figure 4 shows data for the planar second-moment correlation length ξ defined in Eq. (7), for $Z = 5, 9, 13$, and $T \lesssim T_c$. We observe that ξ is small for $T > T_c$, and apparently L and Z independent (for sufficiently large L and Z), indicating that it remains finite in the large-L and large-Z limits. Around T_c the data of ξ appear to converge to a finite value when increasing L at fixed Z; however, they show that ξ increases with increasing Z, approximately as $\xi \sim Z$ at T_c. Then, for sufficiently small values of T, the data begin showing a significant dependence on L. At low temperature we observe $\xi \sim L$ at fixed T, suggesting that ξ diverges with increasing L even when keeping Z fixed. In the following, we show that this apparently complicated behavior can be explained by the DC scenario put forward in the previous section.

To begin with, we investigate the nature of the low-temperature behavior where the planar correlation length ξ appears to diverge with increasing L. At low temperature, BH systems for any thickness Z should show a quasi-2D QLRO phase, whose behavior is essentially described by the 2D spin-wave theory (see in particular Appendix A). As discussed in Appendix A 1, this implies universal relations among the ratio $R_L \equiv \xi/L$, the quasi-2D helicity modulus Y, and the exponent η characterizing the planar two-point correlation function. In Fig. 5 we plot data of R_L versus those of Y, comparing them with the universal curve $\mathcal{R}_L(\mathcal{Y})$ which can be easily obtained from the spin-wave results reported in Appendix A 1. This curve ends at the BKT point $(Y^*, R_L^*) = (0.6365\ldots, 0.7506\ldots)$. For sufficiently small T, depending on the value of Z, the data approach the universal spin-wave curve $\mathcal{R}_L(\mathcal{Y})$ with increasing L. Extrapolations using the expected power-law corrections [cf. Eqs. (A9) and (A10)] turn out to be consistent with the exact spin-wave results. Therefore, the numerical results nicely support the existence of a QLRO phase for any Z, with the expected universal spin-wave behaviors.

We also note that above a given temperature, depending on the thickness Z, the data do not approach the spin-wave curve $\mathcal{R}_L(\mathcal{Y})$ anymore, as it is expected to occur for $T > T_{\rm BKT}$ where both R_L and Y vanish in the large-L limit. Therefore, the data of Fig. 5 allow us to approximately locate $T_{\rm BKT}$ between the temperature values of the data closest to the BKT point (Y^*, R_L^*) which respectively approach the spin-wave curve and deviate from it. We already note that $T_{\rm BKT}$ increases with increasing Z. This can be also inferred from the data of the helicity modulus Y versus the temperature (see Fig. 6). They are generally decreasing, and for sufficiently large T they appear to cross the value $Y = Y^* \approx 0.6365$ corresponding to the BKT transition, indicating that those values of T are larger than $T_{\rm BKT}$.

More accurate estimates of $T_{\rm BKT}$ can be obtained by looking for the optimal values of T achieving the matching of the available data of Y and R_L with the finite-size dependence of the 2D XY model at its BKT transition (see Appendix A 2). In particular, $T_{\rm BKT}(Z)$ is determined by the value of T providing the optimal matching of the data of $Y(Z,L,T)$ with the finite-size dependence of the helicity modulus of the 2D XY model, i.e.,

$$Y(Z,L,T) = \widetilde{Y}_{XY}[\lambda(Z)L] + O(L^{-2}), \qquad (21)$$

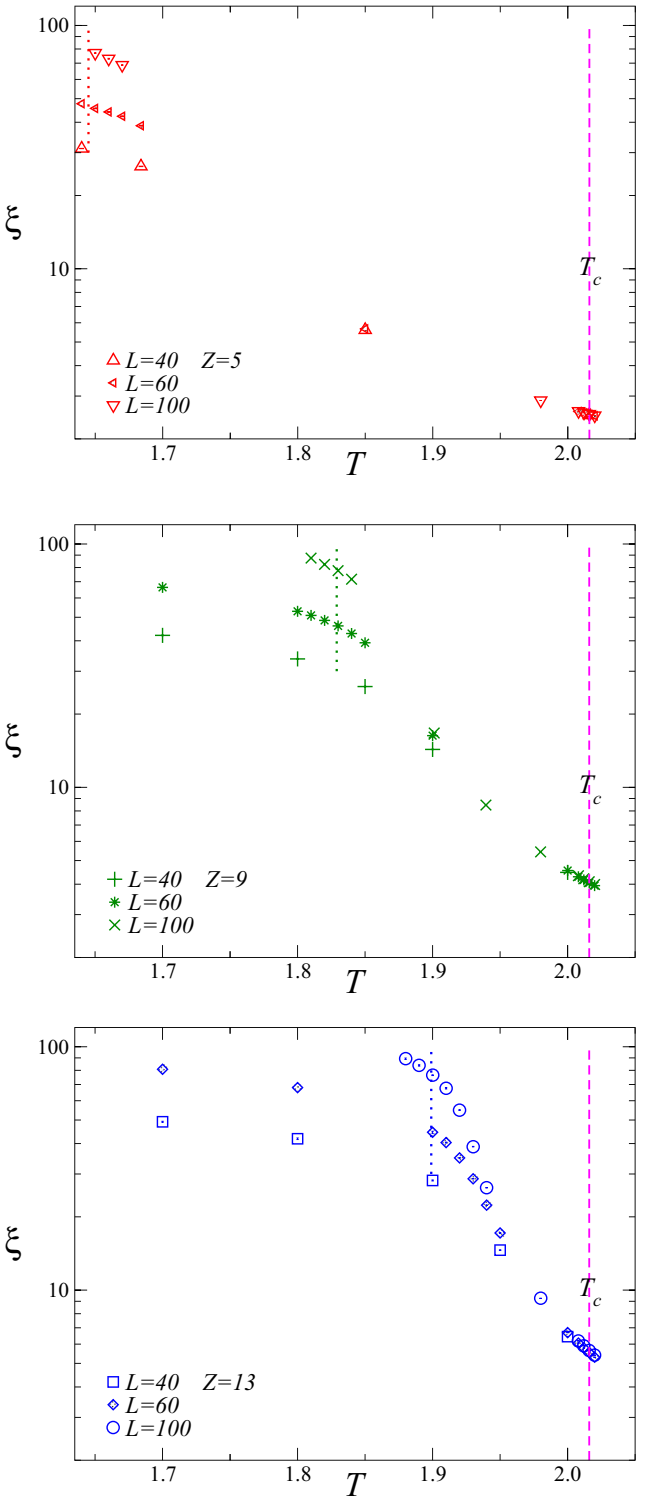

FIG. 4. The planar correlation length ξ vs the temperature T for the hard-core $U \to \infty$ BH model at zero chemical potential. We plot QMC data for $Z = 5$ (top), $Z = 9$ (middle), and $Z = 13$ (bottom). Note that all figures show the same ranges of T and ξ values, to favor the comparison of the data for different thickness Z. Lengths are expressed in units of the lattice spacing, while T is in units of the hopping parameter. The dashed vertical line indicates the BEC transition temperature T_c, the dotted vertical lines indicate our estimates of the Z-dependent BKT transition temperature. The statistical errors of the data are so small to be hardly visible.

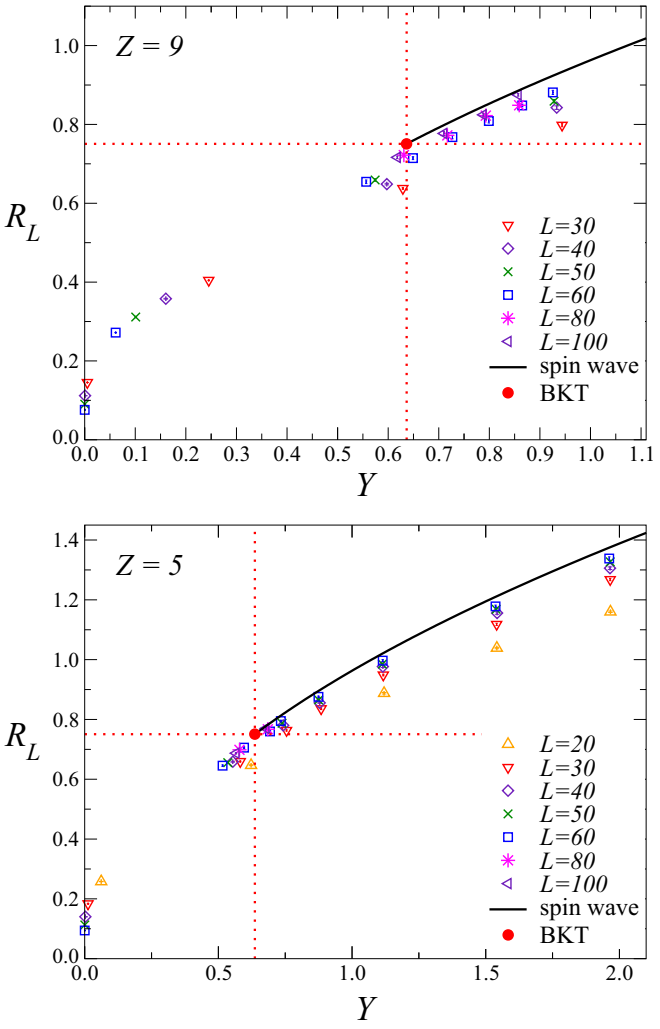

FIG. 5. $R_L \equiv \xi/L$ vs Y for $Z = 5$ (bottom) and $Z = 9$ (top), and for several values of L and T. The full line shows the spin-wave curve $\mathcal{R}_L(\mathcal{Y})$ which is expected to be asymptotically approached for $L \to \infty$ within the QLRO phase; its end point corresponds to the BKT transition. In particular, for $Z = 5$ the values of T of the data shown in the bottom figure are (from right to left) $T = 1.1858$, 1.3518, 1.5179, 1.6, 1.64, 1.65, 1.67, 1.6839, 1.85. The behavior of the data close to the BKT point suggests $T_{\rm BKT}(Z = 5) \approx 1.65$. Analogously for $Z = 9$ the data are for $T = 1.8$, 1.81, 1.82, 1.83, 1.84,1.85, 1.9, 2; they suggest that $T_{\rm BKT}(Z = 9) \approx 1.83$. The statistical errors of the data are so small to be hardly visible.

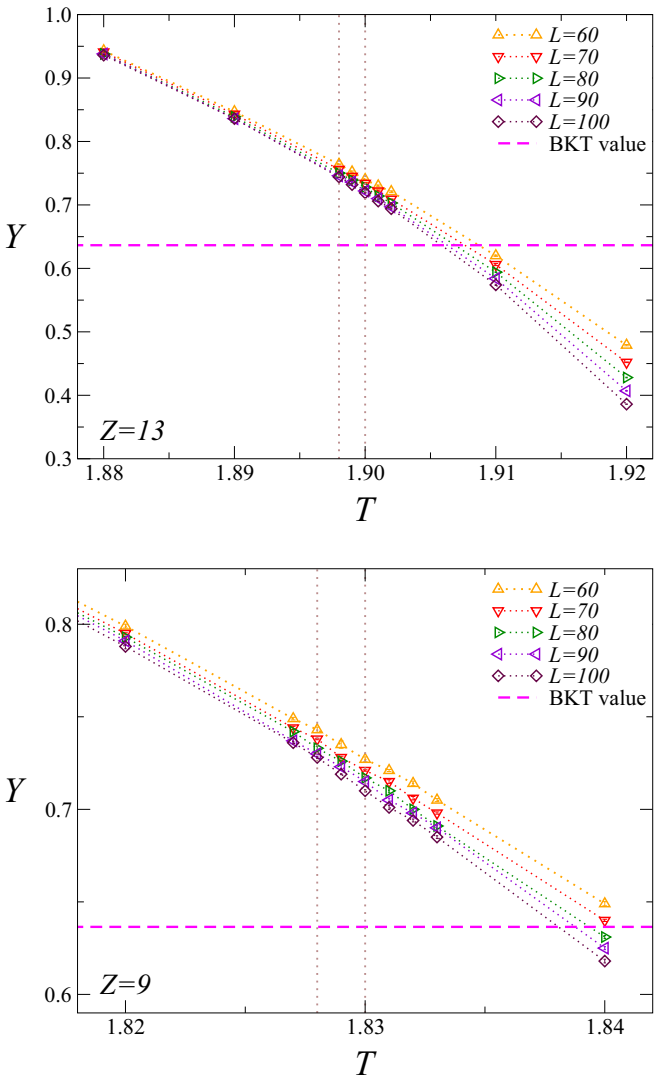

FIG. 6. Data of Y vs T (in units of the hopping parameter), for $Z = 9$ (bottom) and $Z = 13$ (top) around the corresponding BKT temperatures. Analogous results have been obtained for $Z = 5$. The dashed horizontal line indicates the BKT value $Y^* = 0.6365\ldots$. The dotted vertical lines indicate the interval corresponding to our best estimates of $T_{\rm BKT}$, i.e., $T_{\rm BKT} = 1.829(1)$ for $Z = 9$ and $T_{\rm BKT} = 1.899(1)$ for $Z = 13$, obtained by the matching procedure.

with $\widetilde{Y}_{XY}$ given by Eq. (A20). This numerical analysis largely suppresses the systematic error because it is not affected by logarithmic corrections, but only $O(L^{-2})$ power-law corrections. For $Z = 1$ the optimal matching led to the estimate $T_{\rm BKT}(Z = 1) = 0.6877(2)$ and $\lambda(Z = 1) \approx 1.5$.

We determine the optimal values of T and $\lambda(Z)$ satisfying the scaling relation (21). We skip most details of the numerical matching procedures, which can be found in Ref. [73]. We only mention that we use QMC data from $L = 20$ to 100, for sufficiently close values of T, to obtain reliable estimates for any T by interpolation (see Fig. 6). Our estimates for the optimal matching parameters are

$$T_{\rm BKT}(Z = 5) = 1.645(2), \quad T_{\rm BKT}(Z = 9) = 1.829(1),$$
$$T_{\rm BKT}(Z = 13) = 1.899(1). \tag{22}$$

Correspondingly, we obtain $\lambda(Z = 5) = 0.4(2)$, $\lambda(Z = 9) = 0.20(5)$, and $\lambda(Z = 13) = 0.14(2)$. The statistical error of the analysis is estimated using bootstrap methods. The error reported above takes also into account the variations of the results when changing the procedure to obtain the optimal matching, for example, when considering or not the $O(L^{-2})$ scaling corrections, and varying the minimum size L of the data used in the analysis.

The quality of the matching can be appreciated looking at Fig. 7, which shows the data for the optimal matching values of $T_{\rm BKT}$ versus the ratio $L/\Lambda(Z)$ with $\Lambda(Z) = \Lambda_{XY}/\lambda(Z)$, so

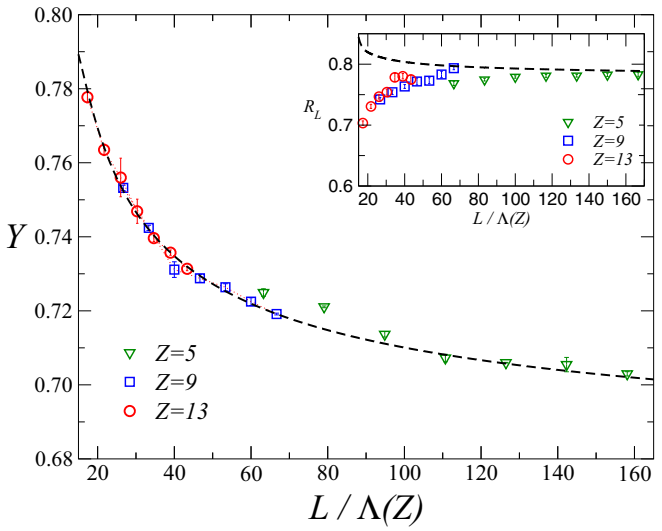

FIG. 7. Finite-size dependence of Y at the BKT transition. We plot data for $Z = 5, 9, 13$ at their best estimates of $T_{\rm BKT}$, i.e., $T = 1.645, 1.829, 1.899$, respectively, versus $L/\Lambda(Z)$ with $\Lambda(Z) = \Lambda_{XY}/\lambda(Z) = 0.6, 1.5, 2.4$, respectively. The dashed line shows the XY curve (A20). The inset shows data of R_L, with the corresponding XY curve (dashed line) taken from Ref. [73].

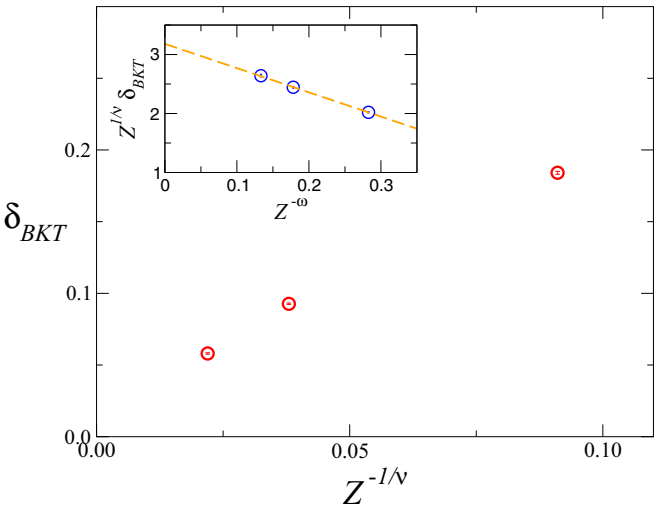

FIG. 8. Estimates of $\delta_{\rm BKT}(Z) \equiv 1 - T_{\rm BKT}(Z)/T_c$ vs $Z^{-1/\nu}$ with $\nu = 0.6717$ (the transverse size is reported in units of the lattice spacing). The data are compatible with the expected behavior $\delta_{\rm BKT}(Z) \sim Z^{-1/\nu}$. The inset shows the product $Z^{1/\nu}\delta_{\rm BKT}(Z)$ vs $Z^{-\omega}$ with $\omega = 0.785$ (the dashed line is obtained by a linear fit), which is the expected behavior of the leading scaling corrections.

that all data of Y, for any Z, are expected to follow the same curve $\widetilde{Y}_{XY}$ versus L/Λ_{XY} with $\Lambda_{XY} = 0.31$. This is indeed what we observe, apart from some scaling corrections at the smallest values of L, which are expected to get suppressed as $O(L^{-2})$. We consider the results of the matching analysis of the Y data as our best estimates of $T_{\rm BKT}$. Note also that the values of $\lambda(Z)$ are decreasing, as expected because the value $\lambda(Z)L$ is somehow related to the equivalent planar size of the lattice, and for a slab geometry one may expect that this is approximately given by the aspect ratio L/Z, thus $\lambda(Z) \sim 1/Z$ roughly.

An analogous numerical analysis can be done using the data of R_L. However, it turns out to be less accurate. As also observed in Ref. [73], R_L is subject to larger power-law scaling corrections, which decrease as $L^{-7/4}$. The XY curve of R_L is reported in Ref. [73]. Note that once $T_{\rm BKT}$ and $\lambda(Z)$ are determined, there are no other free parameters to optimize the matching. The inset of Fig. 7 shows the data and their comparison with the XY curve using the values of $T_{\rm BKT}$ and $\lambda(Z)$ obtained from the analysis of the data of Y. The data appear to approach the asymptotic curve with increasing L, therefore, they are consistent with the theoretical predictions. However, as already mentioned, we note that the approach to the expected asymptotic behavior is characterized by larger scaling corrections, thus requiring larger lattice sizes to obtain independent estimates of $T_{\rm BKT}$ as accurate as those obtained using the data of Y.

Figure 8 shows $\delta_{\rm BKT}(Z) \equiv 1 - T_{\rm BKT}(Z)/T_c$ versus $Z^{-1/\nu}$, as obtained from the above estimates of $T_{\rm BKT}$. The data turn out to be consistent with the expected asymptotic behavior $\delta_{\rm BKT}(Z) \sim Z^{-1/\nu}$. We also estimate

$$X_{\rm BKT} = \lim_{Z\to\infty} Z^{1/\nu}\delta_{\rm BKT} = 3.2(1) \qquad (23)$$

by extrapolating the available data for the product $Z^{1/\nu}\delta_{\rm BKT}$ using the ansatz

$$Z^{1/\nu}\delta_{\rm BKT} = X_{\rm BKT} + c\, Z^{-\omega}, \qquad (24)$$

where $\omega = 0.785(20)$ is the leading scaling-correction exponent of the 3D XY universality class (see the inset of Fig. 8).

Finally, we check the TFSS of R_Z around T_c in the planar thermodynamic limit, i.e., when $\xi, Z \ll L$, reported by Eq. (13). As argued in Sec. III B, the scaling function $f_\xi(X)$ is expected to have an essential singularity at $X_{\rm BKT} \approx 3.2$ [cf. Eq. (14)]. In Fig. 9 we show data of R_Z around T_c

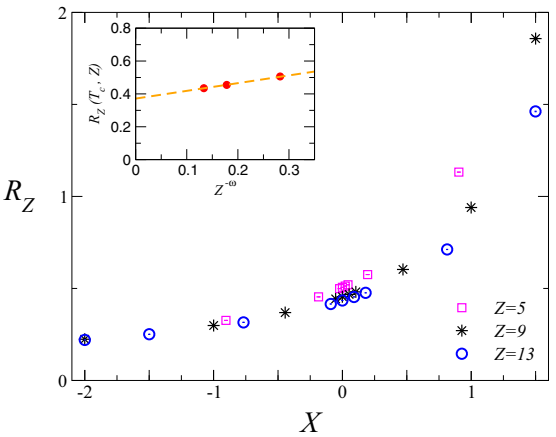

FIG. 9. Scaling of R_Z around T_c. Most data are taken for $L = 120$, which is sufficiently large to provide a good approximation of the $L \to \infty$ limit in the range of Z and X values considered, within about 1%. We plot the data versus $X \equiv Z^{1/\nu}\delta$ with $\nu = 0.6717$ and $\delta \equiv 1 - T/T_c$. The inset shows the data of R_Z at T_c vs $Z^{-\omega}$ which is the expected behavior of the leading scaling corrections (the dashed line is obtained by a linear fit).

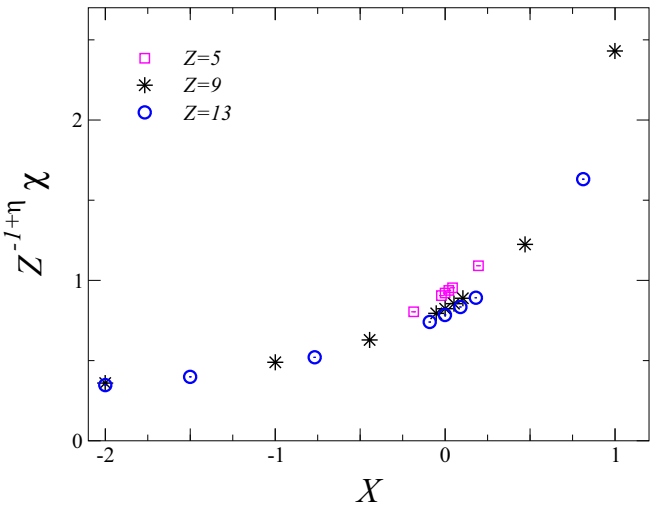

FIG. 10. Scaling of the planar susceptibility χ around T_c. We plot $Z^{-1+\eta}\chi$ vs $X \equiv Z^{1/\nu}\delta$. The data support the asymptotic TFSS $\chi \approx Z^{1-\eta}\mathcal{C}(X)$.

versus $X \equiv \delta Z^{1/\nu}$. They support the TFSS behavior of R_Z. Scaling corrections are expected to decrease as $Z^{-\omega}$. They appear significantly larger for $X > 0$, when approaching the singularity at $X_{\rm BKT}$. By extrapolating the available data at T_c using $R_Z(Z,T_c) = R_Z^* + c\,Z^{-\omega}$ (see the inset of Fig. 9), we estimate $R_Z^* = 0.372(3)$ for the universal large-Z ratio $R_Z \equiv \xi/Z$ characterizing the TFSS of the critical planar correlation length. An analogous scaling behavior is expected for the planar susceptibility defined as in Eq. (5). The data shown in Fig. 10 nicely support the corresponding TFSS relation (19).

V. BOSE GASES CONFINED BY A TRANSVERSE HARMONIC TRAP

We now discuss the case of quasi-2D gases trapped by a harmonic potential along the transverse direction, analogously to the experimental setup of Ref. [31].

A. BH model in a transverse harmonic trap

In the case of the BH model, the presence of a space-dependent trapping potential can be taken into account by adding a further Hamiltonian term to Eq. (1), i.e.,

$$H_{\rm hBH} = H_{\rm BH} + \sum_i V(z_i) n_i, \tag{25}$$

$$V(z) = |z/\ell|^p, \tag{26}$$

where z_i is the distance of the site i from the central plane, $p > 0$, and ℓ can be considered as the transverse trap size. The harmonic potential corresponds to $p = 2$. The transverse trapping potential coupled to the particle density can also be interpreted as an effective chemical-potential parameter depending on the transverse coordinate z,

$$\mu_e(\mu,z) \equiv \mu - V(z). \tag{27}$$

Far from the central $z = 0$ plane, the potential $V(z)$ diverges, thus, $\mu_e \to -\infty$ therefore $\langle n_i \rangle$ vanishes and the particles are trapped along the transverse direction.

We discuss the behavior of the system in the limit of infinite size of the planar dimensions, along which the system appears as homogeneous. For practical realizations, this regime may be realized by considering hard-wall traps along the planar directions with size $L \gg \ell$ (more precisely $L \gg \ell^\theta$ where the exponent $\theta < 1$ is given below), such as the experimental setup of Ref. [31].

The planar correlation functions, for example along the $z = 0$ plane, are expected to behave similarly to the case of transverse hard-wall traps. With decreasing T from the high-temperature normal phase, the length scale ξ gets large around the BEC transition temperature T_c (i.e., the critical temperature of the BEC transition of the corresponding homogeneous 3D system). But, it does not diverge since $\xi \sim \ell^\theta$ where θ is an appropriate exponent (see below). Then, one may observe a BKT transition to a QLRO phase around the $z = 0$ plane, at $T_{\rm BKT} < T_c$ depending on ℓ. In particular, in the extreme $\ell \to 0$ limit, where all particles are confined within the $z = 0$ plane, we recover the homogeneous 2D BH model, i.e., the model (1) with $Z = 1$. On the other hand, in the opposite $\ell \to \infty$ limit, we again expect that $T_{\rm BKT}(\ell) \to T_c^-$, analogously to the homogeneous case. Therefore, similarly to the homogeneous case, the system passes from a high-temperature 3D behavior to a quasi-2D critical behavior at low temperature. This change of regime may be also related to a transverse condensation phenomenon [31,33,38,83,84].

B. Transverse trap-size scaling

Like homogeneous systems with transverse hard-wall boundary conditions, the 3D critical behavior must be somehow recovered in the large-ℓ limit, in a spatial region sufficiently close to the central $z = 0$ plane. We argue that this limit can be described by a universal transverse-trap-size scaling (TTSS), similar to the TFSS limit discussed in Sec. III B. To derive the TTSS laws for the case at hand, we can exploit the same arguments used to derive the trap-size scaling for isotropic or 1D traps [14,24,26,85].

The trapping potential (26) coupled to the particle density significantly affects the critical modes, introducing another length scale ℓ. Like general critical phenomena (see, e.g., Ref. [62]), the asymptotic scaling behavior of the length scale at T_c is expected to be characterized by a power law:

$$\xi_t \sim \ell^\theta. \tag{28}$$

The exponent θ can be determined by a scaling analysis of the perturbation associated with the external potential coupled to the particle density. Its derivation is identical to that reported in Refs. [14,26] for isotropic traps. The exponent θ turns out to be related to the correlation-length exponent ν of the universality class of the critical behavior of the homogeneous BEC transition, i.e.,

$$\theta = \frac{p\nu}{1 + p\nu}, \tag{29}$$

where $\nu = 0.6717(1)$ is the correlation-length exponent of the 3D XY universality class. For harmonic transverse traps, i.e., $p = 2$, $\theta = 0.57327(4)$.

On the basis of these TTSS arguments, we expect that the asymptotic large-ℓ behavior of the two-point function around the central $z = 0$ plane, and in particular the correlation function defined as in Eq. (4), behaves as

$$g(\boldsymbol{x},\ell) \approx \xi_t^{-(1+\eta)} \mathcal{G}_p\left(\boldsymbol{x}/\xi_t, \delta \xi_t^{1/\nu}\right), \tag{30}$$

where $\xi_t \sim \ell^\theta$, $\delta \equiv 1 - T/T_c$, and we have assumed that the planar sizes are infinite. Actually, one may also take into account the planar size L by adding a further scaling variable L/ℓ^θ; the $L \to \infty$ scaling behavior (30) is recovered when $L/\ell^\theta \gg 1$.

The TTSS of the two-point function implies that the planar second-moment correlation length along the $z = 0$ plane, defined as in Eq. (7), behaves asymptotically as

$$\xi_t \approx \ell^\theta \mathcal{R}_p(\mathcal{X}), \quad \mathcal{X} \equiv \delta \ell^{\theta/\nu}. \tag{31}$$

In particular, we recover $\xi_t \sim \ell^\theta$ at T_c. Note that this scaling behavior is analogous to that of the hard-wall traps [cf. Eq. (13)], with the transverse size Z replaced by ℓ^θ. The leading corrections to the above asymptotic TTSS are $O(\ell^{-\omega\theta})$.

Note also that the trap exponent θ reported in Eq. (29) is identical to that of isotropic traps [26], i.e., it does not depend on the number of coordinates entering the space dependence of the inhomogeneous power-law potential coupled to the particle density. However, the scaling functions $\mathcal{G}_p$ and $\mathcal{R}_p$, entering Eqs. (30) and (31), must definitely differ. Actually, in the $p \to \infty$ limit we must recover the TFSS behavior, i.e., that of the homogeneous conditions along the transverse direction with OBC (see Sec. III B). Since $\theta \to 1$ for $p \to \infty$, $\ell \approx Z$ of the transverse hard-wall conditions.

The TTSS functions must present a singularity related to the BKT transition for $T_{\rm BKT} < T_c$, unlike those of the isotropic TSS because no such transition occurs for isotropic traps. In particular, TTSS implies that

$$\delta_{\rm BKT}(\ell) \equiv 1 - T_{\rm BKT}(\ell)/T_c \sim \ell^{-\theta/\nu}, \tag{32}$$

and the TTSS function $\mathcal{R}_p(\mathcal{X})$ of Eq. (31) must show a BKT-like singularity at

$$\mathcal{X}_{\rm BKT} = \lim_{\ell\to\infty} \delta_{\rm BKT}(\ell)\, \ell^{\theta/\nu}, \tag{33}$$

such as that reported in Eq. (14).

We finally mention that other interesting features emerge at the boundary of the BEC region in atomic gases confined by a transverse harmonic trap. If the trap is sufficiently large and the temperature is sufficiently low, i.e., $T < T_c$, different phases may coexist in different space regions, when moving from the central $z = 0$ plane of the trap. Indeed, due to the fact that the effective chemical potential $\mu_e(z)$ [cf. Eq. (27)] decreases with increasing z, the BEC region is generally spatially limited. When moving from the $z = 0$ plane, the quantum gas passes from the BEC phase around the center of the trap (where space coherence is essentially described by spin waves) to a normal phase far from the center. The gas is expected to develop a peculiar critical behavior at the boundary of the BEC region, with a nontrivial scaling behavior controlled by the universality class of the homogenous BEC transition in the presence of an effective linear external potential coupled to the particle density [32]. Some details are reported in Appendix B.

VI. OFF-EQUILIBRIUM SLOW DYNAMICS AND DIMENSIONAL CROSSOVER

The dynamical behavior of statistical systems driven across phase transitions is a typical off-equilibrium phenomenon. Indeed, the large-scale modes present at the transition are unable to reach equilibrium as the system changes phase, even when the time scale t_s of the variation of the system parameters is very large. Such phenomena are of great interest in many different physical contexts, at both first-order and continuous transitions, where one may observe hysteresis and coarsening phenomena, the Kibble-Zurek (KZ) defect production, etc. (see, e.g., Refs. [30,33,59,60,86–97]). The correlation functions obey general off-equilibrium scaling (OS) laws in the limit of large time scale t_s of the variations across the transition, which are controlled by the universal static and dynamic exponents of the equilibrium transition [89,91,97].

We now consider the off-equilibrium behavior arising from slow time variations of the temperature T across the BEC transition. We assume a standard linear protocol, varying T so that

$$\delta(t) \equiv 1 - T(t)/T_c = t/t_s, \tag{34}$$

starting at a time $t_i < 0$ in the high-T phase and ending at $t_f > 0$ in the low-T phase. t_s is the time scale of the temperature variation. The BEC transition point corresponds to $t = 0$ (however, this is not strictly required, it is only convenient for our discussion). Several experiments implementing off-equilibrium time-dependent protocols in cold-atom systems have been reported (see, e.g., Refs. [30,31,33,98–100]).

Aside from the static critical exponent [64] $\nu = 0.6717(1)$ of the 3D XY universality class, we also need information on the critical dynamic behavior at the BEC transition. This is characterized by the dynamic exponent $z = d/2$, thus $z = \frac{3}{2}$ in 3D, associated with the model-F dynamics [101,102] which is conjectured to describe the dynamic universality class of the 3D BEC transition.

In the standard thermodynamic limit of cubiclike boxes, with $L_1 \sim L_2 \sim L_3 \sim L$ and $L \to \infty$, one defines the OS limit as the large-time-scale limit $t_s \to \infty$, keeping the OS scaling variables

$$\mathcal{T} \equiv t/t_s^\kappa, \quad \boldsymbol{x}_s \equiv \boldsymbol{x}/t_s^\zeta \tag{35}$$

fixed. Scaling arguments allow us to determine the appropriate exponents κ and ζ, obtaining [59,60,91]

$$\kappa = \frac{z\nu}{1+z\nu}, \quad \zeta = \frac{\nu}{1+z\nu}, \tag{36}$$

where ν and z are the static correlation-length and dynamic exponents. In particular, by inserting the known values of ν and z, we obtain $\kappa = 0.50188(4)$ and $\zeta = 0.33459(3)$.

We may apply these OS arguments to the equal-time two-point correlation function, measured after a time t and averaged over the initial Gibbs distribution at a given initial temperature

$T > T_c$. Standard scaling arguments lead to the OS asymptotic behaviors [91]

$$G(\boldsymbol{x},t,t_s) \approx t_s^{-\zeta(1+\eta)} \mathcal{G}_o(\boldsymbol{x}_s,\mathcal{T}). \tag{37}$$

Moreover, we expect

$$\xi(t,t_s) \approx t_s^{\zeta}\, \mathcal{R}_o(\mathcal{T}) \tag{38}$$

for any length scale associated with the critical modes. Experimental studies of this dynamic behavior, and the related KZ defect production, led to the estimate [30] $\zeta = 0.35(4)$, which is in good agreement with the theoretical result (36).

We now discuss how this off-equilibrium behavior may change in quantum gases confined within a slab geometry with $Z \ll L$, and in particular with a finite thickness Z and infinite $L \to \infty$ planar sizes. Analogous experiments with quasi-2D cold-atom systems constrained in a slab geometry have been reported in Refs. [31,33] (homogeneous hard-wall traps along the planar directions and harmonic along the transverse direction). They observe the emergence of coherence when cooling the atomic gas through the BEC temperature.

The off-equilibrium behavior arising from the slow variation of the temperature across the BEC transition point is made particularly complex by the presence of the quasi-2D BKT transition. Thus, disentangling the behaviors corresponding to BEC and BKT is quite hard in experimental or numerical analyses. The authors of [31,33] interpreted the observed behavior as a transverse condensation phenomenon [31,33,83,84]. In the following, we put forward an alternative framework to describe the DC in a slab geometry, based on an off-equilibrium FSS (OFSS).

As already said, for a finite thickness Z, even though $L \to \infty$, the system does not develop a diverging correlation length at the 3D BEC transition temperature T_c, but ξ remains of the order of the transverse size Z. Thus, the systems can evolve adiabatically, i.e., its evolution can be performed by passing through quasiequilibrium states for a sufficiently large time scale t_s of the variation of $T(t)$ around T_c. This is possible until it reaches the BKT transition at the time $t > 0$ corresponding to $T_{\rm BKT}$, i.e., when $t/t_s = \delta_{\rm BKT} \equiv 1 - T_{\rm BKT}/T_c$.

Of course, the OS at the BKT transition is expected to substantially differ from that at the 3D BEC transition, such as Eqs. (37) and (38), because it must be controlled by the 2D universality class of the BKT transition in quantum gases. At the BKT transition the relevant exponents for KZ off-equilibrium protocols are expected to be $\nu = \infty$ (related to the exponential increase of the correlation length when $T \to T_{\rm BKT}^{+}$) and $z = 1$ (2D model F of the dynamics). Thus, the power laws of the off-equilibrium scaling variables (35) at the BKT transition lead to $\kappa = 1$, apart from logarithms.

However, things become quite involved when the thickness Z becomes large because the BKT transition gets very close to the BEC temperature T_c [cf. Eq. (15)]. Therefore, the analysis of numerical and experimental data may become hard, and straightforward power-law fits may turn out to be misleading.

In order to describe the time-dependent DC of a slab geometry under the protocol (34), we consider an OFSS framework involving the size Z of the transverse direction. The appropriate OFSS limit is defined by introducing the scaling variables

$$X_o = Z^{1/\nu}\delta(t), \quad W_o = Z^{-1/\zeta} t_s. \tag{39}$$

The OFSS limit of the planar correlation length defined in Eq. (7) is expected to be described by the scaling relation

$$\xi(Z,t,t_s) \approx Z\, \mathcal{S}_o(X_o,W_o), \tag{40}$$

where $\mathcal{S}_o$ is a universal OFSS function.

In this OS framework, the equilibrium FSS around T_c is recovered in the limit $W_o \to \infty$, i.e.,

$$\mathcal{S}_o(X_o, W_o \to \infty) = \mathcal{R}(X_o), \tag{41}$$

where $\mathcal{R}(X_o)$ is the equilibrium FSS function [cf. Eq. (13)]. In particular, at $t = 0$ corresponding to $T(t) = T_c$, we expect to recover the equilibrium result $\xi \sim Z$ when $t_s \gg Z^{1/\zeta}$. Note, however, that the equilibrium limit is not well defined for any X_o because it diverges when $X_o \geqslant X_{\rm BKT}$ [cf. Eq. (16)], corresponding to the BKT transition. Around $X_{\rm BKT}$ the behavior of the scaling functions must somehow show the off-equilibrium singularities associated with a slow passage through a BKT transition.

The above scaling behaviors can be straightforwardly extended to the case of a transverse harmonic trap, using the same TTSS arguments of Sec. V. Apart from replacing Z with ℓ^{θ}, the main features of the OS behavior remain the same.

We mention that experiments under analogous time-dependent protocols crossing the BEC transition have been performed with atomic gases confined in slablike traps with a transverse harmonic trapping potential [31,33]. They were able to check the initial 3D behavior, without a clear identification of the subsequent quasi-2D behavior. The computation of the defect production arising from the KZ mechanism is further complicated by later-time coarsening phenomena [87,91,93].

VII. SUMMARY

We have studied the phase-coherence properties of Bose gases confined within slablike boxes of size $L^2 \times Z$ with $Z \ll L$, at the 3D BEC transition temperature T_c and at lower temperatures. Unlike systems confined within cubiclike geometries, i.e., boxes with $L \sim Z$, the low-temperature behavior of gases confined within a slab geometry is also characterized by the possibility of undergoing a finite-temperature quasi-2D BKT transition at $T_{\rm BKT} < T_c$ with $T_{\rm BKT}$ depending on the thickness Z. Below $T_{\rm BKT}$ the planar one-particle correlations decay algebraically, as predicted by the QLRO of the 2D spin-wave theory.

Therefore, Bose gases in a slab geometry experience DC with decreasing T, from 3D behaviors for $T \gtrsim T_c$ to a quasi-2D critical behavior for $T \lesssim T_{\rm BKT}$. However, in the limit of large thickness Z the quasi-2D BKT transition temperature approaches that of the 3D BEC transition, i.e., $T_{\rm BKT} \to T_c$ for $Z \to \infty$. The interplay of 3D and quasi-2D critical modes can be described by the TFSS limit for systems on a slab geometry: $Z \to \infty$ and $T \to T_c$ keeping the product $(T - T_c)Z^{1/\nu}$ fixed (the planar sizes are assumed to be infinite), where ν is the correlation-length exponent at the 3D BEC transition. The corresponding TFSS functions must present an essential singularity due to the quasi-2D BKT transition below T_c. A similar TTSS behavior is also put forward in the case the

particles are trapped by a transverse harmonic potential in the limit of large transverse trap size ℓ. In the TTSS framework, the length scale $\xi_t = \ell^\theta$, where $\theta = 2\nu/(1+2\nu) = 0.57327(4)$, plays the same role of the transverse size Z of the TFSS.

To provide evidence of the DC scenario in interacting bosonic gases, we present a numerical study of the BH model (1) in anisotropic slablike lattices $L^2 \times Z$ with $Z \ll L$. With decreasing T from the high-temperature normal phase, we first observe a quasi-BEC transition where the critical length scale ξ gets large, but it does not diverge, being limited by $\xi \sim Z$ (keeping Z fixed). Then, a BKT transition occurs to a QLRO phase, where the system develops planar critical correlations essentially described by the 2D Gaussian spin-wave theory. We show that the 3D $\to$ 2D DC scenario explains the apparently complex dependence on T, Z, and L of the one-particle correlation functions and the corresponding length scale, when decreasing the temperature from $T > T_c$ to $T < T_{\rm BKT} < T_c$. The results turn out to be consistent with the predictions of the TFSS at the BEC transition.

The DC scenario is expected to apply to any quantum gas of interacting bosonic particles constrained in boxes or lattice structures with slab geometry. Analogous arguments apply to ^{4}He systems in film geometries [54], and to 3D XY spin models defined in lattices with slab geometries [55–58]. We also mention that some issues related to DC in quasi-2D nonrelativistic boson systems have been also investigated in Ref. [103], in particular the dependence of the 2D superfluid critical temperature on the transverse size in the case of periodic boundary conditions along the transverse direction.

We also extend the discussion to off-equilibrium phenomena of interacting Bose gases confined in a slab geometry, arising from slow time variations of the temperature T across the BEC transition. In particular, we consider the linear protocol $\delta(t) \equiv 1 - T(t)/T_c = t/t_s$ where t_s is a time scale. The corresponding off-equilibrium behavior is made particularly complex by the presence of the close quasi-2D BKT transition at $T_{\rm BKT} < T_c$, which is also crossed during the time-dependent protocol. Thus, disentangling the behaviors corresponding to BEC and BKT is quite hard in experimental or numerical analyses. We argue that the off-equilibrium behavior in the limit of large t_s can be described by an off-equilibrium FSS theory for bosonic gases confined within a slab geometry, extending the TFSS of the equilibrium properties.

We conclude stressing that the above issues related to the DC scenario are of experimental relevance since cold-atom systems confined within slab geometries can be effectively realized (see, e.g., Refs. [28,30,31,33]). These experimental setups offer the possibility of investigating the dependence of the phase-coherence properties on the geometry of the cold-atom system. Our study provides a framework to interpret the experimental or numerical data related to the 3D $\to$ 2D DC of Bose gases confined within slab geometries, and in particular their complicated dependence on the thickness Z.

APPENDIX A: LOW-TEMPERATURE BEHAVIOR OF QUASI-2D BOSONIC GASES

We present some exact results which are expected to characterize the low-temperature QLRO phase of quasi-2D interacting bosonic gases up to the BKT transition.

1. QLRO phase below the BKT transition

The universal features of the QLRO phase of quasi-2D systems with a U(1) symmetry are described by the Gaussian spin-wave theory

$$H_{\rm sw} = \frac{\beta}{2} \int d^2x \, (\nabla\varphi)^2. \tag{A1}$$

For $\beta \geqslant 2/\pi$, corresponding to values $0 \leqslant \eta \leqslant \frac{1}{4}$ for the exponent of the power-law decay of the two-point function, this spin-wave theory describes the QLRO phase. The values $\beta = 2/\pi$ and $\eta = \frac{1}{4}$ correspond to the BKT transition [104].

The spin-wave correlation function

$$G_{\rm sw}(\boldsymbol{x}_1 - \boldsymbol{x}_2) = \langle e^{-i\varphi(\boldsymbol{x}_1)} e^{i\varphi(\boldsymbol{x}_2)} \rangle \tag{A2}$$

is expected to provide the asymptotic large-L behavior of the two-point function of 2D interacting bosonic gases within the QLRO phase. For $|\boldsymbol{x}_1 - \boldsymbol{x}_2| \ll L$,

$$G_{\rm sw}(\boldsymbol{x}_1, \boldsymbol{x}_2) \sim \frac{1}{|\boldsymbol{x}_1 - \boldsymbol{x}_2|^\eta}, \tag{A3}$$

where the exponent η is related to the coupling β by

$$\eta = \frac{1}{2\pi\beta}. \tag{A4}$$

The general size dependence of $G_{\rm sw}$ on a square L^2 box with PBC is also known [73,104–106]:

$$\begin{aligned} G_{\rm sw}(\boldsymbol{x}, L) &= C(\boldsymbol{x}, L)^\eta \times E(\boldsymbol{x}, L), \\ C(\boldsymbol{x}, L) &= \frac{e^{\pi y_2^2} \theta_1'(0, e^{-\pi})}{|\theta_1[\pi(y_1 + i y_2), e^{-\pi}]|}, \\ E(\boldsymbol{x}, L) &= \frac{\sum_{n_1,n_2=-\infty}^{\infty} W(n_1,n_2) \cos[2\pi(n_1 x_1 + n_2 x_2)]}{\sum_{n_1,n_2=-\infty}^{\infty} W(n_1,n_2)}, \\ W(n_1,n_2) &= \exp\left[-\pi \left(n_1^2 + n_2^2\right)/\eta \right], \end{aligned} \tag{A5}$$

where $\boldsymbol{x} \equiv (x_1, x_2)$, $y_i \equiv x_i/L$, $\theta_1(u,q)$ and $\theta_1'(u,q)$ are θ functions [107].

Using Eq. (A5), one can easily compute the universal large-L relation $\mathcal{R}_L(\eta)$ between $R_L \equiv \xi/L$ and η, where ξ is the second-moment correlation length defined as

$$\xi^2 = \frac{L^2}{4\pi^2} \left(\frac{\chi}{\chi_1} - 1 \right), \tag{A6}$$

where

$$\begin{aligned} \chi &= \int d^2x \, G_{\rm sw}(\boldsymbol{x}), \\ \chi_1 &= \int d^2x \cos\left(\frac{2\pi x_1}{L} \right) G_{\rm sw}(\boldsymbol{x}). \end{aligned} \tag{A7}$$

Analogous results are obtained for the helicity modulus [106]

$$\Upsilon(\eta) = \frac{1}{2\pi\eta} - \frac{\sum_{n=-\infty}^{\infty} n^2 \exp(-\pi n^2/\eta)}{\eta^2 \sum_{n=-\infty}^{\infty} \exp(-\pi n^2/\eta)}. \tag{A8}$$

The above asymptotic large-L behaviors (at fixed T or η) are approached with power-law corrections, indeed

$$R_L(L,\eta) \equiv \xi/L = \mathcal{R}_L(\eta) + aL^{-\varepsilon}, \tag{A9}$$

$$Y(L,\eta) = \mathcal{Y}(\eta) + aL^{-\zeta}, \tag{A10}$$

respectively, where ε and ζ are the exponents associated with the expected leading corrections [108,109]:

$$\varepsilon = \mathrm{Min}[2-\eta,\kappa], \quad \zeta = \mathrm{Min}[2,\kappa], \tag{A11}$$

$$\kappa = 1/\eta - 4 + O[(1/\eta - 4)^2]. \tag{A12}$$

With increasing T within the QLRO phase, the critical exponent η of the two-point function [cf. Eq. (A3)] increases up to $\eta = \frac{1}{4}$ corresponding to the BKT transition. Therefore, close to the BKT transition, i.e., for $T \lesssim T_{\rm BKT}$, we may expand the universal curves $\mathcal{R}_L(\eta)$ and $\mathcal{Y}(\eta)$ around $\eta = \frac{1}{4}$, obtaining

$$\mathcal{R}_L(\eta) = 0.7506912222 + 1.699451\left(\frac{1}{4} - \eta\right) + \cdots, \tag{A13}$$

$$\mathcal{Y}(\eta) = 0.6365081782 + 2.551196\left(\frac{1}{4} - \eta\right) + \cdots. \tag{A14}$$

We expect that the above universal behaviors are also realized in the low-temperature phase of BH models within a slab geometry, for $T < T_{\rm BKT}$, by the two-point functions $g(\boldsymbol{x})$ [cf. Eq. (4)] and the quantities $R_L \equiv \xi/L$ and Y defined in Eq. (9).

2. Finite-size behavior at the BKT transition

The BKT transition is characterized by logarithmic corrections to the asymptotic behavior, due to the presence of marginal renormalization-group (RG) perturbations at the BKT fixed point [106,108,110–113]. The asymptotic behaviors at the BKT transition for R_L and Y can be obtained by replacing [106,108]

$$1/4 - \eta \approx \frac{1}{8w}, \quad w = \ln\frac{L}{\Lambda} + \frac{1}{2}\ln\ln\frac{L}{\Lambda} \tag{A15}$$

into Eqs. (A13) and (A14). The nonuniversal details that characterize the model (such as the thickness Z of the quasi-2D BH models) are encoded in the model-dependent scale Λ. Thus, one obtains the asymptotic large-L behavior

$$R(L,T_{\rm BKT}) = R^* + C_R w^{-1} + O(w^{-2}) \tag{A16}$$

for both $R = Y$, R_L, with

$$Y^* = 0.6365081789, \quad C_Y = 0.31889945, \tag{A17}$$

$$R_L^* = 0.7506912222, \quad C_{R_L} = 0.21243137 \tag{A18}$$

for PBC.

In numerical analyses, Eq. (A16) may be used to locate the BKT transition point, i.e., by requiring that the finite-size dependence of the data matches it. However, we note that this straightforward approach is subject to systematic errors which get suppressed only logarithmically with increasing L. This makes the accuracy of the numerical or experimental determination of the critical parameters quite problematic. This problem can be overcome by the so-called matching method [58,73,106,111,112,114,115], which allows us to control the whole pattern of the logarithmic corrections, leaving only power-law corrections.

The matching method exploits the fact that the finite-size behavior of RG invariant quantities R, such as R_L and Y, of different models at their BKT transition shares the same logarithmic corrections apart from a nonuniversal normalization of the scale. Indeed, the L dependence of two models at their BKT transition is related by the asymptotic relation

$$R^{(1)}\big(L_1, T^{(1)}_{\rm BKT}\big) \approx R^{(2)}\big(L_2 = \lambda L_1, T^{(2)}_{\rm BKT}\big), \tag{A19}$$

apart from power-law corrections, which are $O(L^{-2})$ for the helicity modulus Y and $O(L^{-7/4})$ for the ratio R_L. The matching parameter λ is the only free parameter, but it does not depend on the particular choice of the RG invariant quantity. The matching method consists in finding the optimal value of T matching the finite-size behavior of Y and R_L of the 2D XY model whose value of $T_{\rm BKT}$ is known with high accuracy [106,112]. The complete expression of R_L and Y of the 2D XY model have been numerically obtained by high-precision numerical studies [106,114] and by extrapolations using RG results for the asymptotic behavior. For example, the L dependence of the helicity modulus Y at the BKT transition of the 2D XY model is accurately reconstructed by the following expression [29]:

$$\begin{aligned}\widetilde{Y}_{XY}(L) \equiv Y_{XY}(T_{\rm BKT},L) &= 0.6365081782 \\ &+ 0.318899454\, w^{-1} + 2.0319176\, w^{-2} \\ &- 40.492461\, w^{-3} + 325.66533\, w^{-4} \\ &- 874.77113\, w^{-5} + 8.43794\, L^{-2} \\ &+ 79.1227\, L^{-4} - 210.217\, L^{-6},\end{aligned} \tag{A20}$$

where w is given in Eq. (A15) with $\Lambda = \Lambda_{XY} = 0.31$.

The matching method has been already applied [73] to the 2D BH models (1), obtaining the accurate estimate $T_{\rm BKT} = 0.6877(2)$ in the hard-core $U \to \infty$ limit and at half-filling ($\mu = 0$).

APPENDIX B: CRITICALITY AT THE BOUNDARY OF THE BEC REGION IN BOSE GASES TRAPPED BY A TRANSVERSE HARMONIC POTENTIAL

Due to the fact that the effective chemical potential $\mu_e(z)$ [cf. Eq. (27)] decreases with increasing z, the BEC region in the presence of a transverse harmonic trap is generally spatially limited. When moving from the $z = 0$ plane, the quantum gas passes from the BEC phase around the center of the trap (where space coherence is essentially described by spin waves) to a normal phase far from the center. The atomic gas develops a critical behavior at the boundary of the BEC region, with a nontrivial scaling behavior controlled by the universality class of the homogeneous BEC transition in the presence of an effective linear external potential coupled to the particle density. This occurs around the planes where the distance $|z|$ from the $z = 0$ plane is such that $T[\mu_e(\mu,z)]$ is equal to the BEC transition temperature at the local chemical potential

$\mu_e(\mu,z) = \mu - (z/\ell)^2$, i.e., when

$$T_c[\mu_e(\mu,z)] \approx T < T_c(\mu). \tag{B1}$$

For example, consider the hard-core BH lattice gas (25) for $\mu \leqslant 0$ and $T < T_c(\mu)$ (see Fig. 1). Since $T_c(\mu)$ decreases with decreasing μ, a plane exists at distance $z = z_b$ such that $T_c[\mu_e(\mu,z_b)] = T$, thus,

$$z_b = \ell\sqrt{\mu - \bar{\mu}}, \tag{B2}$$

where $T_c(\bar{\mu}) = T$. This plane separates the superfluid region from the normal-fluid region. As argued in Ref. [32], in the limit of large ℓ, the correlation functions around the surface where $T_c[\mu_e(\boldsymbol{r})] = T$ are expected to develop a peculiar critical behavior in the presence of an external effectively linear potential coupled to the particle density. The scaling behavior around the critical plane $z = z_b$ can be derived using the same arguments of Ref. [32], applying them to the particular case of a slab geometry where the harmonic potential is only applied along the transverse direction, while the system is translationally invariant along the planar directions.

Around $z = z_b$,

$$V(z) = V(z_b) + \Delta z/\ell_b + O[(\Delta z/\ell_b)^2] \tag{B3}$$

with

$$\ell_b = \frac{\ell}{2\sqrt{\mu - \bar{\mu}}}. \tag{B4}$$

The critical behavior at the critical planes $z = z_b$ is essentially determined by the linear term

$$V_b = \Delta z/\ell_b, \quad \Delta z \equiv z - z_b, \tag{B5}$$

where ℓ_b provides the length scale of the spatial variation. High-order terms of the expansion of the potential around z_b do not affect the asymptotic behavior [32]. Since $\sqrt{\mu - \bar{\mu}} > 0$ is assumed finite and fixed, $\ell_b \sim \ell$. Of course, an analogous behavior occurs on the opposite side, i.e., for $z = -z_b$. The system develops critical correlations around the planes $z = z_b$, with a length scale

$$\xi_b \sim \ell_b^{\theta_b}, \quad \theta_b = \frac{\nu}{1+\nu} = 0.40181(3). \tag{B6}$$

For example, the one-particle correlation function along a transverse direction is expected to scale as

$$G[(\boldsymbol{x},z_1),(\boldsymbol{x},z_2)] \approx \xi_b^{-1-\eta}\mathcal{G}_b(\Delta z_1/\xi_b, \Delta z_2/\xi_b). \tag{B7}$$

Of course, such a scaling behavior at the critical planes is anisotropic, distinguishing the planar and transverse directions. However, both length scales along planar and transverse directions are expected to scale as $\ell_b^{\theta_b}$.

[1] E. A. Cornell and C. E. Wieman, Nobel Lecture: Bose-Einstein condensation in a dilute gas, the first 70 years and some recent experiments, Rev. Mod. Phys. **74**, 875 (2002); N. Ketterle, Nobel lecture: When atoms behave as waves: Bose-Einstein condensation and the atom laser, *ibid.* **74**, 1131 (2002).

[2] M. R. Andrews, C. G. Townsend, H.-J. Miesner, D. S. Durfee, D. M. Kurn, and W. Ketterle, Observation of interference between two bose condensates, Science **275**, 637 (1997).

[3] J. Stenger, S. Inouye, A. P. Chikkatur, D. M. Stamper-Kurn, D. E. Pritchard, and W. Ketterle, Bragg Spectroscopy of a Bose-Einstein Condensate, Phys. Rev. Lett. **82**, 4569 (1999).

[4] E. W. Hagley, L. Deng, M. Kozuma, M. Trippenbach, Y. B. Band, M. Edwards, M. Doery, P. S. Julienne, K. Helmerson, S. L. Rolston, and W. D. Phillips, Measurement of the Coherence of a Bose-Einstein Condensate, Phys. Rev. Lett. **83**, 3112 (1999).

[5] I. Bloch, T. W. Hänsch, and T. Esslinger, Measurement of the spatial coherence of a trapped Bose gas at the phase transition, Nature (London) **403**, 166 (2000).

[6] S. Dettmer, D. Hellweg, P. Ryytty, J. J. Arlt, W. Ertmer, K. Sengstock, D. S. Petrov, G. V. Shlyapnikov, H. Kreutzmann, L. Santos, and M. Lewenstein, Observation of phase fluctuations in Elongated Bose-Einstein Condensates, Phys. Rev. Lett. **87**, 160406 (2001).

[7] D. Hellweg, S. Dettmer, P. Ryytty, J. J. Arlt, W. Ertmer, K. Sengstock, D. S. Petrov, G. V. Shlyapnikov, H. Kreutzmann, L. Santos, and M. Lewenstein, Phase Fluctuations in Bose-Einstein Condensates, Appl. Phys. B **73**, 781 (2001).

[8] D. Hellweg, L. Cacciapuoti, M. Kottke, T. Schulte, K. Sengstock, W. Ertmer, and J. J. Arlt, Measurement of the Spatial Correlation Function of Phase Fluctuating Bose-Einstein Condensates, Phys. Rev. Lett. **91**, 010406 (2003).

[9] S. Ritter, A. Öttl, T. Donner, T. Bourdel, M. Köhl, and T. Esslinger, Observing the Formation of Long-Range Order during Bose-Einstein Condensation, Phys. Rev. Lett. **98**, 090402 (2007).

[10] I. Bloch, J. Dalibard, and W. Zwerger, Many-body physics with ultracold gases, Rev. Mod. Phys. **80**, 885 (2008).

[11] T. Donner, S. Ritter, T. Bourdel, A. Öttl, M. Köhl, and T. Esslinger, Critical behavior of a trapped interacting Bose gas, Science **315**, 1556 (2007).

[12] R. B. Diener, Q. Zhou, H. Zhai, and T. L. Ho, Criterion for Bosonic Superfluidity in an Optical Lattice, Phys. Rev. Lett. **98**, 180404 (2007).

[13] A. Bezett and P. B. Blakie, Critical properties of a trapped interacting Bose gas, Phys. Rev. A **79**, 033611 (2009).

[14] M. Campostrini and E. Vicari, Critical Behavior and Scaling in Trapped Systems, Phys. Rev. Lett. **102**, 240601 (2009); Erratum: Critical Behavior and Scaling in Trapped Systems [Phys. Rev. Lett. **102**, 240601 (2009)] **103**, 269901(E) (2009); Trap-size scaling in confined particle systems at quantum transitions, Phys. Rev. A **81**, 023606 (2010).

[15] Q. Zhou, Y. Kato, N. Kawashima, and N. Trivedi, Direct Mapping of the Finite Temperature Phase Diagram of Strongly Correlated Quantum Models, Phys. Rev. Lett. **103**, 085701 (2009).

[16] S. Trotzky, L. Pollet, F. Gerbier, U. Schnorrberger, I. Bloch, N. V. Prokofev, B. Svistunov, and M. Troyer, Suppression of the critical temperature for superfluidity near the Mott transition, Nat. Phys. **6**, 998 (2010).

[17] T.-L. Ho and Q. Zhou, Obtaining the phase diagram and thermodynamic quantities of bulk systems from the densities of trapped gases, Nat. Phys. **6**, 131 (2010).
[18] L. Pollet, N. V. Prokof'ev, and B. V. Svistunov, Criticality in Trapped Atomic Systems, Phys. Rev. Lett. **104**, 245705 (2010).
[19] S. Nascimbene, N. Nayon, F. Chevy, and C. Salomon, The equation of state of ultracold Bose and Fermi gases: A few examples, New J. Phys. **12**, 103026 (2010).
[20] Q. Zhou, Y. Kato, N. Kawashima, and N. Trivedi, Direct Mapping of the Finite Temperature Phase Diagram of Strongly Correlated Quantum Models, Phys. Rev. Lett. **105**, 199601 (2010).
[21] S. L. A. de Queiroz, R. R. dos Santos, and R. B. Stinchcombe, Finite-size scaling behavior in trapped systems, Phys. Rev. E **81**, 051122 (2010).
[22] S. Fang, C-M. Chung, P-N. Ma, P. Chen, and D-W. Wang, Quantum criticality from in situ density imaging, Phys. Rev. A **83**, 031605(R) (2011).
[23] K. R. A. Hazzard and E. J. Mueller, Techniques to measure quantum criticality in cold atoms, Phys. Rev. A **84**, 013604 (2011).
[24] L. Pollet, Recent developments in quantum Monte Carlo simulations with applications for cold gases, Rep. Prog. Phys. **75**, 094501 (2012).
[25] J. Carrasquilla and M. Rigol, Superfluid to normal phase transition in strongly correlated bosons in two and three dimensions, Phys. Rev. A **86**, 043629 (2012).
[26] G. Ceccarelli, C. Torrero, and E. Vicari, Critical parameters from trap-size scaling in trapped particle systems, Phys. Rev. B **87**, 024513 (2013).
[27] G. Ceccarelli and J. Nespolo, Universal scaling of three-dimensional bosonic gases in a trapping potential, Phys. Rev. B **89**, 054504 (2014).
[28] L. Corman, L. Chomaz, T. Bienaimé, R. Desbuquois, C. Wettenberg, S. Nascimbene, J. Dalibard, and J. Beugnon, Quench-Induced Supercurrents in an Annular Bose Gas, Phys. Rev. Lett. **113**, 135302 (2014).
[29] G. Ceccarelli, J. Nespolo, A. Pelissetto, and E. Vicari, Bose-Einstein condensation and critical behavior of two-component bosonic gases, Phys. Rev. A **92**, 043613 (2015); Phase diagram and critical behaviors of mixtures of Bose gases, **93**, 033647 (2016).
[30] N. Navon, A. L. Gaunt, R. P. Smith, and Z. Hadzibabic, Critical dynamics of spontaneous symmetry breaking in a homogeneous bose gas, Science **347**, 167 (2015).
[31] L. Chomaz, L. Corman, T. Bienaimé, R. Desbuquois, C. Wettenberg, S. Nascimbene, J. Beugnon, and J. Dalibard, Emergence of coherence via transverse condensation in a uniform quasi-two-dimensional Bose gas, Nat. Commun. **6**, 6162 (2015).
[32] F. Delfino and E. Vicari, Critical behavior at the spatial boundary of a trapped inhomogeneous Bose-Einstein condensate, Phys. Rev. A **95**, 053606 (2017).
[33] J. Beugnon and N. Navon, Exploring the Kibble-Zurek mechanism with homogeneous Bose gases, J. Phys. B: At., Mol. Opt. Phys. **50**, 022002 (2017).
[34] G. Ceccarelli, F. Delfino, M. Mesiti, and E. Vicari, Shape dependence and anisotropic finite-size scaling of the phase coherence of three-dimensional Bose-Einstein condensed gases, Phys. Rev. A **94**, 053609 (2016).
[35] D. S. Petrov, G. V. Shlyapnikov, and J. T. M. Walraven, Phase-Fluctuating 3D Bose-Einstein Condensates in Elongated Traps, Phys. Rev. Lett. **87**, 050404 (2001).
[36] L. Mathey, A. Ramanathan, K. C. Wright, S. R. Muniz, W. D. Phillips, and C. W. Clark, Phase fluctuations in anisotropic Bose-Einstein condensates: From cigars to rings, Phys. Rev. A **82**, 033607 (2010).
[37] D. Gallucci, S. P. Cockburn, and N. P. Proukakis, Phase coherence in quasicondensate experiments: An *ab initio* analysis via the stochastic Gross-Pitaevskii equation, Phys. Rev. A **86**, 013627 (2012).
[38] W. RuGway, A. G. Manning, S. S. Hodgman, R. G. Dall, A. G. Truscott, T. Lamberton, and K. V. Kheruntsyan, Observation of Transverse Bose-Einstein Condensation via Hanbury Brown-Twiss Correlations, Phys. Rev. Lett. **111**, 093601 (2013).
[39] J. M. Kosterlitz and D. J. Thouless, Ordering, metastability and phase transitions in two-dimensional systems, J. Phys. C: Solid State Phys. **6**, 1181 (1973).
[40] V. L. Berezinskii, Destruction of Long-range Order in One-dimensional and Two-dimensional Systems having a Continuous Symmetry Group I. Classical Systems, Zh. Eksp. Theor. Fiz. **59**, 907 (1970) [Sov. Phys. JETP **32**, 493 (1971)].
[41] J. M. Kosterlitz, The critical properties of the two-dimensional xy model, J. Phys. C: Solid State Phys. **7**, 1046 (1974).
[42] J. V. José, L. P. Kadanoff, S. Kirkpatrick, and D. R. Nelson, Renormalization, vortices, and symmetry-breaking perturbations in the two-dimensional planar model, Phys. Rev. B **16**, 1217 (1977).
[43] Z. Hadzibabic, P. Krüger, M. Cheneau, B. Battelier, and J. Dalibard, Berezinskii-Kosterlitz-Thouless crossover in a trapped atomic gas, Nature (London) **441**, 1118 (2006).
[44] P. Krüger, Z. Hadzibabic, and J. Dalibard, Critical Point of an Interacting Two-Dimensional Atomic Bose Gas, Phys. Rev. Lett. **99**, 040402 (2007).
[45] Z. Hadzibabic, P. Krüger, M. Cheneau, S. P. Rath, and J. Dalibard, The trapped two-dimensional Bose gas: From Bose-Einstein condensation to Berezinskii-Kosterlitz-Thouless physics, New J. Phys. **10**, 045006 (2008).
[46] P. Cladé, C. Ryu, A. Ramanathan, K. Helmerson, and W. D. Phillips, Observation of a 2D Bose Gas: From Thermal to Quasicondensate to Superfluid, Phys. Rev. Lett. **102**, 170401 (2009).
[47] C.-L. Hung, X. Zhang, N. Gemelke, and C. Chin, Observation of scale invariance and universality in two-dimensional Bose gases, Nature (London) **470**, 236 (2011).
[48] T. Plisson, B. Allard, M. Holzmann, G. Salomon, A. Aspect, P. Bouyer, and T. Bourdel, Coherence properties of a two-dimensional trapped Bose gas around the superfluid transition, Phys. Rev. A **84**, 061606(R) (2011).
[49] R. Desbuquois, L. Chomaz, T. Ysefsah, J. Léonard, J. Beugnon, C. Weitenberg, and J. Dalibard, Superfluid behavior of a two-dimensional Bose gas, Nat. Phys. **8**, 645 (2012).
[50] M. N. Barber, Finite-size scaling, in *Phase Transitions and Critical Phenomena*, Vol. 8, edited by C. Domb and J. L. Lebowitz (Academic, New York, 1983).
[51] *Finite Size Scaling and Numerical Simulations of Statistical Systems*, edited by V. Privman (World Scientific, Singapore, 1990).

[52] M. P. A. Fisher, P. B. Weichman, G. Grinstein, and D. S. Fisher, Boson localization and the superfluid-insulator transition, Phys. Rev. B **40**, 546 (1989).

[53] D. Jaksch, C. Bruder, J. I. Cirac, C. W. Gardiner, and P. Zoller, Cold Bosonic Atoms in Optical Lattices, Phys. Rev. Lett. **81**, 3108 (1998).

[54] F. M. Gasparini, M. O. Kimball, K. P. Mooney, and M. Diaz-Avilla, Finite-size scaling of ^{4}He at the superfluid transition, Rev. Mod. Phys. **80**, 1009 (2008).

[55] N. Schultka and E. Manousakis, Crossover from two- to three-dimensional behavior in superfluids, Phys. Rev. B **51**, 11712 (1995).

[56] N. Schultka and E. Manousakis, Scaling of superfluid density in superfluid films, J. Low Temp. Phys. **105**, 3 (1996).

[57] N. Schultka and E. Manousakis, Boundary effects in superfluid films, J. Low Temp. Phys. **109**, 733 (1997).

[58] M. Hasenbusch, The Kosterlitz-Thouless transition in thin films: A Monte Carlo study of three-dimensional lattice models, J. Stat. Mech.: Theory Exp. (2009) P02005.

[59] T. W. B. Kibble, Topology of cosmic domains and strings, J. Phys. A: Math. Gen. **9**, 1387 (1976).

[60] W. H. Zurek, Cosmological experiments in superfluid helium? Nature (London) **317**, 505 (1985).

[61] B. Capogrosso-Sansone, N. V. Prokof'ev, and B. V. Svistunov, Phase diagram and thermodynamics of the three-dimensional Bose-Hubbard model, Phys. Rev. B **75**, 134302 (2007).

[62] A. Pelissetto and E. Vicari, Critical phenomena and renormalization group theory, Phys. Rep. **368**, 549 (2002).

[63] J. A. Lipa, D. R. Swanson, J. A. Nissen, T. C. P. Chui, and U. E. Israelsson, Heat Capacity and Thermal Relaxation of Bulk Helium Very Near the Lambda Point, Phys. Rev. Lett. **76**, 944 (1996); J. A. Lipa, J. A. Nissen, D. A. Stricker, D. R. Swanson, and T. C. P. Chui, Specific heat of liquid helium in zero gravity very near the lambda point, Phys. Rev. B **68**, 174518 (2003).

[64] M. Campostrini, M. Hasenbusch, A. Pelissetto, and E. Vicari, Theoretical estimates of the critical exponents of the superfluid transition in ^{4}He by lattice methods, Phys. Rev. B **74**, 144506 (2006).

[65] E. Burovski, J. Machta, N. Prokof'ev, and B. Svistunov, High-precision measurement of the thermal exponent for the three-dimensional XY universality class, Phys. Rev. B **74**, 132502 (2006).

[66] R. Guida and J. Zinn-Justin, Critical exponents of the N-vector model, J. Phys. A: Math. Gen. **31**, 8103 (1998).

[67] F. Kos, D. Poland, D. Simmons-Duffin, and A. Vichi, Precision Islands in the Ising and O(N) Models, J. High Energy Phys. 08 (2016) 036.

[68] M. V. Kompaniets and E. Panzer, Minimally subtracted six loop renormalization of O(n)-symmetric φ^4 theory and critical exponents, Phys. Rev. D **96**, 036016 (2017).

[69] M. E. Fisher, M. N. Barber, and D. Jasnow, Helicity modulus, superfluidity, and scaling in isotropic systems, Phys. Rev. A **8**, 1111 (1973).

[70] E. L. Pollock and D. M. Ceperley, Path-integral computation of superfluid densities, Phys. Rev. B **36**, 8343 (1987).

[71] N. D. Mermin and H. Wagner, Absence of Ferromagnetism or Antiferromagnetism in One- or Two-Dimensional Isotropic Heisenberg Model, Phys. Rev. Lett. **17**, 1133 (1966).

[72] P. C. Hohenberg, Existence of long-range order in one and two dimensions, Phys. Rev. **158**, 383 (1967).

[73] G. Ceccarelli, J. Nespolo, A. Pelissetto, and E. Vicari, Universal behavior of two-dimensional bosonic gases at Berezinskii-Kosterlitz-Thouless transitions, Phys. Rev. B **88**, 024517 (2013).

[74] K. Harada and N. Kawashima, Universal jump in the helicity modulus of the two-dimensional quantum XY model, Phys. Rev. B **55**, R11949 (1997).

[75] H.-Q. Ding, Phase transition and thermodynamics of quantum XY model in two dimensions, Phys. Rev. B **45**, 230 (1992).

[76] H.-Q. Ding and M. S. Makivić, Kosterlitz-Thouless transition in the two-dimensional quantum XY model, Phys. Rev. B **42**, 6827 (1990).

[77] M. E. Fisher, in *Critical Phenomena, Proceedings of the International School of Physics Enrico Fermi*, edited by M. S. Green (Academic, New York, 1971).

[78] T. W. Capehart and M. E. Fisher, Susceptibility scaling functions for ferromagnetic Ising films, Phys. Rev. B **13**, 5021 (1976).

[79] V. Ambegaokar, B. I. Halperin, D. R. Nelson, and E. D. Siggia, Dynamics of superfluid films, Phys. Rev. B **21**, 1806 (1980).

[80] A. W. Sandvik and J. Kurlijärvi, Quantum Monte Carlo simulation method for spin systems, Phys. Rev. B **43**, 5950 (1991).

[81] O. F. Syljuåsen and A. W. Sandvik, Quantum Monte Carlo with directed loops, Phys. Rev. E **66**, 046701 (2002).

[82] A. Dorneich and M. Troyer, Accessing the dynamics of large many-particle systems using the stochastic series expansion, Phys. Rev. E **64**, 066701 (2001).

[83] N. J. van Druten and W. Ketterle, Two-Step Condensation of the Ideal Bose Gas in Highly Anisotropic Traps, Phys. Rev. Lett. **79**, 549 (1997).

[84] J. Armjio, T. Jacqmin, K. Kheruntsyan, and I. Bouchoule, Mapping out the quasicondensate transition through the dimensional crossover from one to three dimensions, Phys. Rev. A **83**, 021605 (2011).

[85] A. Angelone, M. Campostrini, and E. Vicari, Universal quantum behaviors of interacting fermions in 1D traps: From few particles to the trap thermodynamic limit, Phys. Rev. A **89**, 023635 (2014).

[86] K. Binder, Theory of first-order phase transitions, Rep. Prog. Phys. **50**, 783 (1987).

[87] A. J. Bray, Theory of phase-ordering kinetics, Adv. Phys. **43**, 357 (1994).

[88] P. Calabrese and A. Gambassi, Ageing Properties of Critical Systems, J. Phys. A: Math. Gen. **38**, R133 (2005).

[89] S. Gong, F. Zhong, X. Huang, and S. Fan, Finite-time scaling via linear driving, New J. Phys. **12**, 043036 (2010).

[90] A. Polkovnikov, K. Sengupta, A. Silva, and M. Vengalattore, Colloquium: Nonequilibrium dynamics of closed interacting quantum systems, Rev. Mod. Phys. **83**, 863 (2011).

[91] A. Chandran, A. Erez, S. S. Gubser, and S. L. Sondhi, Kibble-Zurek problem: Universality and the scaling limit, Phys. Rev. B **86**, 064304 (2012).

[92] S. Braun, M. Friesdorf, S. S. Hodgman, M. Schreiber, J. P. Ronzheimer, A. Riera, M. del Rey, I. Bloch, J. Eisert, and U. Schneider, Emergence of coherence and the dynamics of

quantum phase transitions, Proc. Natl. Acad. Sci. USA **112**, 3641 (2015).
[93] G. Biroli, Slow Relaxations and Non-Equilibrium Dynamics in Classical and Quantum Systems, arXiv:1507.05858.
[94] A. Pelissetto and E. Vicari, Off-equilibrium scaling behaviors driven by time-dependent external fields in three-dimensional O(N) vector models, Phys. Rev. E **93**, 032141 (2016).
[95] M. J. Davis, T. M. Wright, T. Gasenzer, S. A. Gardiner, and N. P. Proukakis, Formation of Bose-Einstein condensates, arXiv:1601.06197.
[96] M. Anquez, B. A. Robbins, H. M. Bharath, M. J. Boguslawski, T. M. Hoang, and M. S. Chapman, Kibble-Zurek Mechanism in a Spin-1 Bose-Einstein Condensate, Phys. Rev. Lett. **116**, 155301 (2016).
[97] A. Pelissetto and E. Vicari, Dynamic Off-Equilibrium Transition in Systems Slowly Driven Across Thermal First-Order Transitions, Phys. Rev. Lett. **118**, 030602 (2017).
[98] L. E. Sadler, J. M. Higbie, S. R. Leslie, M. Vengalattore, and D. M. StamperKurn, Spontaneous symmetry breaking in a quenched ferromagnetic spinor Bose-Einstein condensate, Nature (London) **443**, 312 (2006).
[99] C. N. Weiler, T. W. Neely, D. R. Scherer, A. S. Bradley, M. J. Davis, and B. P. Anderson, Spontaneous vortices in the formation of Bose-Einstein condensates, Nature (London) **455**, 948 (2008).
[100] G. Lamporesi, S. Donadello, S. Serafini, F. Dalfovo, and G. Ferrari, Spontaneous creation of Kibble-Zurek solitons in a Bose-Einstein condensate, Nat. Phys. **9**, 656 (2013).
[101] P. C. Hohenberg and B. I. Halperin, Theory of dynamic critical phenomena, Rev. Mod. Phys. **49**, 435 (1977).
[102] R. Folk and G. Moser, Critical dynamics: A field-theoretical approach, J. Phys. A: Math. Gen. **39**, R207 (2006).
[103] S. Lammers, I. Boettcher, and C. Wetterich, Dimensional crossover of nonrelativistic bosons, Phys. Rev. A **93**, 063631 (2016).
[104] C. Itzykson and J. M. Drouffe, *Statistical Field Theory* (Cambridge University Press, Cambridge, 1989).
[105] P. Di Francesco, P. Mathieu, and D. Senechal, *Conformal Field Theory* (Springer, New York, 1997).
[106] M. Hasenbusch, The two dimensional XY model at the transition temperature: A high precision numerical study, J. Phys. A: Math. Gen. **38**, 5869 (2005).
[107] I. S. Gradshteyn and I. M. Ryzhik, in *Table of Integrals, Series, and Products*, edited by A. Jeffrey and D. Zwillinger, 7th ed. (Academic, San Diego, 2007).
[108] A. Pelissetto and E. Vicari, Renormalization-group flow and asymptotic behaviors at the Berezinskii-Kosterlitz-Thouless transitions, Phys. Rev. E **87**, 032105 (2013).
[109] M. Hasenbusch, A. Pelissetto, and E. Vicari, Multicritical behavior in the fully frustrated XY model and related systems, J. Stat. Mech.: Theory Exp. (2005) P12002.
[110] D. J. Amit, Y. Y. Goldschmidt, and G. Grinstein, Renormalisation group analysis of the phase transition in the 2D Coulomb gas, Sine-Gordon theory and XY-model, J. Phys. A: Math. Gen. **13**, 585 (1980).
[111] M. Hasenbusch, M. Marcu, and K. Pinn, High precision renormalization group study of the roughening transition, Phys. A (Amsterdam) **208**, 124 (1994).
[112] M. Hasenbusch and K. Pinn, Computing the roughening transition of Ising and solid-on-solid models by BCSOS model matching, J. Phys. A: Math. Gen. **30**, 63 (1997).
[113] J. Balog, Kosterlitz-Thouless theory and lattice artifacts, J. Phys. A: Math. Gen. **34**, 5237 (2001).
[114] M. Hasenbusch, The Binder cumulant at the Kosterlitz-Thouless transition, J. Stat. Mech.: Theory Exp. (2008) P08003.
[115] M. Hasenbusch, Thermodynamic Casimir effect: Universality and corrections to scaling, Phys. Rev. B **85**, 174421 (2012).